






Wetland Change Analysis in Alberta, Canada Using Four Decades of Landsat Imagery

Meisam Amani , Senior Member, IEEE, Sahel Mahdavi , Mohammad Kakooei , Arsalan Ghorbanian , Brian Brisco , Evan R. DeLancey, Souleymane Toure, and Eugenio Landeiro Reyes

Abstract—In this study, wetland trends in Alberta were investigated in the past four decades using Landsat satellite imagery to produce updated information about wetland changes and to prevent further degradation of these valuable natural resources. All the processing steps and analyses were conducted in Google earth engine (GEE) to produce 16 wetland maps from 1984 to 2020. A comprehensive change analysis showed 1) approximately 18% of the province was subjected to change; 2) in terms of wetland classes, there was a decreasing trend for the Shallow Water and Swamp classes and an increasing trend for the Fen and Marsh classes; 3) in terms of nonwetland classes, there was a considerable decreasing trend for the Forest class and increasing trend for the Grassland/Shrubland class; 4) wetland loss was approximately 22 000 km², which was mainly due to the conversion of wetlands to Forest and Grassland/Shrubland; 5) wetland gain was approximately 24 000 km², which was mainly due to the conversion from the Forest class to wetlands, especially the Swamp and Fen classes; 6) the highest class transition was from Cropland to Grassland/Shrubland and vice versa (29 000 km²), from Forest to different wetland classes (18 000 km²), and from Fen to Forest (6000 km²). In summary, the results of this study provided the first comprehensive information on wetland trends in Alberta over the past 37 years and will assist policymakers to adjust the required/established policies to mitigate the potential wetland changes due to anthropogenic activities and climate-related events.

Index Terms—Big data, change detection (CD), cloud computing, Google earth engine (GEE), Landsat, machine learning, random forest (RF), remote sensing (RS), wetland.

Manuscript received May 27, 2021; revised July 12, 2021 and August 23, 2021; accepted August 26, 2021. Date of publication September 8, 2021; date of current version October 21, 2021. This research was funded by Environment and Climate Change Canada under Grant to Dr. Meisam Amani. (Corresponding author: Meisam Amani.)

Meisam Amani and Sahel Mahdavi are with the Wood Environment and Infrastructure Solutions, Ottawa, ON K2E 7L5, Canada (e-mail: meisam.amani@woodplc.com; sahel.mahdavi@woodplc.com).

Mohammad Kakooei is with the Department of Electronic Engineering, Babol Noshiravani University of Technology, Babol 4714871167, Iran (e-mail: kakooei.mohammad@stu.nit.ac.ir).

Arsalan Ghorbanian is with the Department of Photogrammetry and Remote Sensing, Faculty of Geodesy and Geomatics Engineering, K. N. Toosi University of Technology, Tehran 1969764499, Iran (e-mail: a.ghorbanian@email.kntu.ac.ir).

Brian Brisco is with the Canada Center for Mapping and Earth Observation, Ottawa, ON K1S 5K2, Canada. (e-mail: brian.brisco@canada.ca).

Evan R. DeLancey is with the Alberta Biodiversity Monitoring Institute, University of Alberta, Edmonton, AB T6G 2E9, Canada (e-mail: edelance@ualberta.ca).

Souleymane Toure and Eugenio Landeiro Reyes are with the Environment and Climate Change Canada, Gatineau, QC K1A 0H3, Canada (e-mail: souleymane.toure@canada.ca; eugenio.landeiroreyes@canada.ca).

Digital Object Identifier 10.1109/JSTARS.2021.3110460

I. INTRODUCTION

WETLANDS provide diverse benefits to the environment and are valuable habitats for numerous types of flora and fauna. For instance, they clean water, prevent flooding, and preserve soil [1], [2]. Wetlands, especially peatlands (i.e., bogs and fens), are also important sources of carbon emission and contain approximately 35% of the world's terrestrial carbon [3]. However, these advantages were not well understood until recent years, after a vast portion of wetlands were destroyed and/or altered due to various human activities, such as urbanization, resource development, agricultural lands expansion, as well as intense irrigation and ground water extraction [4], [5]. Additionally, climate change exacerbates wetlands degradation by exerting a negative impact on the functionality of wetlands, leading to changes in wetlands ecosystem [6]. Therefore, it is important to assess the wetland changes over time and the reasons behind them using advanced technologies, such as remote sensing (RS) techniques. These analyses will help to make efficient policies to conserve wetlands.

RS can assist in wetland change analysis by providing a rich archive of a variety of datasets and offering numerous advanced change detection (CD) algorithms. For example, launching the first Earth observation (EO) satellite in the Landsat series dates back to 1972. Currently, not only Landsat-7 and Landsat-8 satellites are still operational, but also an extensive record of the Landsat images covering several previous decades exists. More importantly, Landsat images, along with several other types of RS datasets, are freely available, making change analysis more cost-effective. However, this requires processing a large amount of RS data. For instance, if the objective is wetland CD in a large area (e.g., nation-wide) over several decades, thousands of satellite images should be processed in a computation-efficient approach. Therefore, an effective big data processing platform, such as Google earth engine (GEE), is required for these types of tasks [7], [8].

GEE is a big geo-data processing platform developed by Google in 2010. This cloud computing platform efficiently addresses the challenges of analyzing and prototyping big geospatial data using parallel processing. Moreover, GEE offers a variety of built-in codes, including preprocessing and classification algorithms, which allow users to generate the desired products with minimal effort [7], [8]. The rich archive EO datasets within GEE makes it particularly useful for long-term CD [9]. Since its development, GEE has been used in a variety of disciplines, such as Land Cover/Land Use (LCLU) classification [10]–[13], agriculture [14], [15], soil mapping

[16], urban mapping and monitoring [17], glacier studies [18], water detection and monitoring [19], [20], atmosphere and climate analysis [21], [22], and LCLU CD [9], [23], [24]. There are a significant number of studies that have used GEE for long-term change analysis. For example, Midekisa *et al.* [25] identified the land cover changes in the continental Africa over 15 years using Landsat images in the GEE platform. Furthermore, Shimizu *et al.* [26] used a combination of Landsat-8 and Sentinel-1 time series to detect disturbances in tropical forests in Myanmar during 2014 and 2018. Chen *et al.* [23] also investigated the changes in coastal wetlands and the effect of reclamation in China's Yellow Sea during 1984 and 2015. They found out that the areas of coastal wetlands decreased by 53%. Additionally, Huang *et al.* [27] analyzed the changes in green spaces of 28 cities during 10 years (2005–2015) within GEE. The authors reported approximately 4% and 7% increases in the availability and accessibility of the green spaces, respectively. Finally, Mahdianpari *et al.* [9] analyzed wetland changes over Newfoundland, Canada using 30-years Landsat data within GEE. They observed the instability of wetland classes over this period and argued that the changes were mainly due to conversion from one wetland class to another.

Numerous CD algorithms have been so far proposed, which could be widely divided into supervised and unsupervised methods [28]–[31]. Supervised CD methods require samples with labels from the classes present in the study area, while unsupervised methods can be applied without having field samples. Although using unsupervised methods eliminates the requirement to conduct field work, these methods do not provide as much information as supervised methods [32]. In other terms, CD techniques can be widely divided into preclassification and postclassification methods. Postclassification techniques consist of creating the map two or more times and then, comparing those maps to detect the areas of change. One limiting factor in postclassification CD techniques is that the accuracy of the change results has a direct relationship with the accuracy of each of the produced maps. However, these methods have the advantage of providing explicit labels for the type of changes [33], [34]. On the other hand, the preclassification CD techniques compare the original images acquired on two or more dates and yield CD maps. These maps typically show the degree of change and need to be binarized to accurately demonstrate the areas of change and no change [35]. Some well-known preclassification CD techniques include principal component analysis and change vector analysis (CVA).

A large portion of Canada is covered by wetlands, which have been degraded over the years. This degradation is more serious in the Alberta province due to natural resource development, several wildfires, and oil and gas activities. For example, it has been reported that as much as 64% of wetlands in Alberta's White Area have been drained and lost [36]. Several studies have so far been conducted to monitor and quantify wetland changes in Alberta over relatively small regions [37]–[40]. For instance, Gillanders *et al.* [38] employed seven Landsat images to investigate the land cover changes in a small area of the Athabasca Oil Sand region between 1989 and 2005. To this end, the Iterative Self-Organizing Data Analysis unsupervised classification method was applied to divide the images into 25 clusters. Later, the EO for Sustainable Development of Forest

land cover product was adopted to label each cluster. Finally, the results revealed that more than 300 km² vegetated land covers were disappeared due to mine activities. In another study, Clare and Creed [39] studied wetland changes and degradations in the Beaverhill subwatershed in central Alberta. Two wetland inventory maps of 1999 and 2009 were first produced through object-based classification of aerial photographs and Light Detection and Ranging (LiDAR) data, respectively. Then, the two maps were subtracted to analyze the changes between these two years. It was reported that over 240 wetland sites, covering an area of 71 hectares were lost due to the land cover transition of wetlands to developed (i.e., urban and industrial) and agricultural areas. Furthermore, orthophoto mosaics, high-resolution satellite images (i.e., GEOEYE1 and WorldView2), and field-collected data were utilized in [40] to map wetland changes in Suncor Base Plant, north of Fort McMurray, Alberta, between 2007 and 2015. Finally, 11 potential zones were manually and visually delineated for CD analysis to reveal wetland reclamation in mining areas using the topographic wetness index in [37]. The analysis indicated that approximately 210 ha of wetlands was spontaneously developed on reclaimed upland landforms.

Although several studies were carried out to map wetland changes in Alberta, they were conducted using relatively traditional methods and within small time intervals and areas. Managers and stakeholders still need reliable wetland data to properly track past and future changes to wetland habitat over the entire province. Doing this needs a long history of the previous data, state-of-the-art image classification, and CD algorithms, as well as powerful big data processing platforms. Therefore, in this study, machine learning classification and CD algorithms were investigated to comprehensively investigate the wetland changes over the past four decades. To this end, the archived Landsat imagery within the GEE platform was employed. This study provides the first comprehensive investigation of wetland changes in the province of Alberta over the past 37 years. The possible reasons behind these changes are also provided to improve the conservation and sustainable management of these valuable natural resources.

The rest of this article is organized as follows. In Section II, the descriptions of the study area, satellite data, and the reference samples, which were used to train the algorithms and evaluate the accuracy of the results, are described. Section III comprehensively discusses the proposed methods for reference samples refinement, wetland classification, and change analysis. In Section IV, the results of classification and CD are discussed. Finally, in Section V, the suggestions for future studies are provided.

II. STUDY AREA AND DATA

A. Study Area

The study area is the entire province of Alberta, Canada, with an area of ~661 848 km² (see Fig. 1). Fig. 1(c) also shows the location of the three oil sand regions in which most of the land cover changes were expected to occur. Alberta has six ecosystem types, including Boreal, Canadian Shield, Foothills, Grassland, Parkland, and Rocky Mountain Natural Regions [41]. Among these regions, the Boreal Forest has the largest area, covering approximately 58% of the province [42]. Each of the

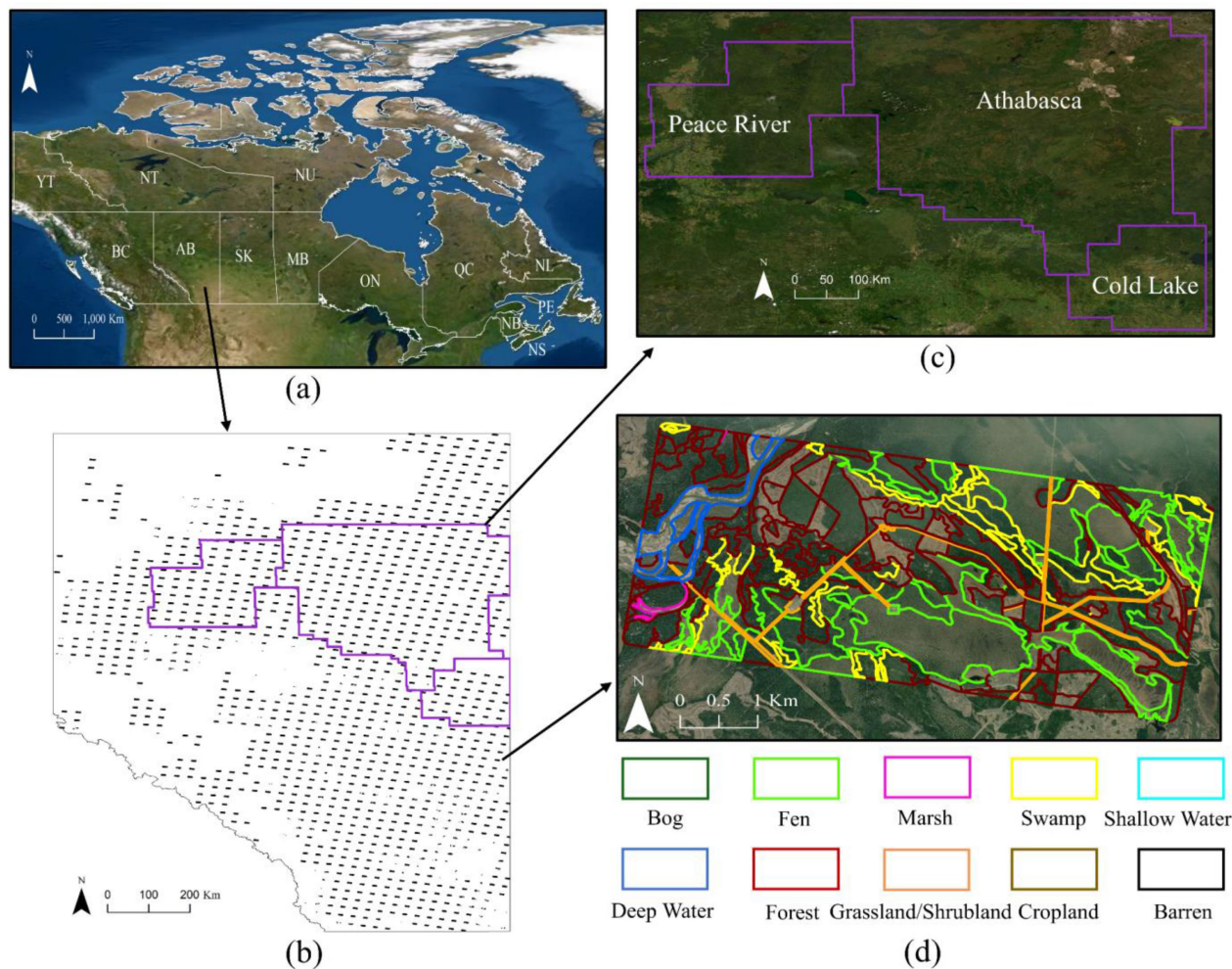


Fig. 1. (a) Canada, (b) Alberta (study area), and the distribution of reference data with the black color. Purple boundaries show the location of oil sands regions. (c) Three oil sands of the Athabasca, Peace River, and Cold Lake. (d) Zoomed image from one of the sample plots.

Alberta's natural regions and subregions is characterized by various species, which are thoroughly described in Downing and Pettapiece [43]. The maximum and minimum elevations in this province are 3747 m and 170 m above sea level in the Rocky Mountains and the Wood Buffalo National Park, respectively [44]. This much elevation difference in the province inevitably creates a considerable variation in the climate [44].

It was reported that almost 21% of the province is covered by wetlands [45]. More than 90% of these wetlands are peatlands (i.e., Bog and Fen) and Swamp. Nonpeatland wetlands (e.g., Marsh and Shallow Water) are also frequently found in Alberta [45]. Therefore, wetlands in Alberta correspond to the Canadian Wetland Classification System (CWCS, [46]), which classifies Canadian wetlands into five classes of Bog, Fen, Marsh, Swamp, and Shallow Water.

B. Reference Data

In Alberta, there is a grid of photo-interpretation plots (each 3×7 km) at the space of 20 km throughout the province [see Fig. 1(b) and (d)], which are generated by the Alberta Biodiversity Monitoring Institute. Wetland types within each plot were classified by interpreting ~ 0.5 m spatial resolution

3-D imagery [42]. In this study, these reference samples were used to train the classifier and validate the produced wetland maps.

Table I provides the information about the number and area of samples available from different years. The wetland classes specified by the CWCS along with the following five main nonwetland classes were considered in the classifications and change analyses: Deep Water (i.e., open water with the depth of more than 2 m), Forest (deciduous, coniferous, and mixed woodlands), Grassland/Shrubland, Cropland, and Barren (i.e., urban, rock, bare soil, sand, and other nonvegetated areas).

In this study, all the 10 wetland and non-wetland classes (called Category-1) were also merged into two additional categories (i.e., Category-2 and Category-3) for further change analysis. Table II demonstrates the classes of each category.

C. Satellite Data

In this study, the archived Landsat-5, -7, and -8 images, available in GEE,¹ were used (see Table III). These images were

¹[Online]. Available: <https://developers.google.com/earth-engine/datasets/catalog/landsat>

TABLE I
NUMBER (AREA/KM²) OF SAMPLE POLYGONS FOR THE WETLAND AND NONWETLAND CLASSES AT DIFFERENT YEARS

Class	2008	2010	2011	2012	2013	2016	Total
Bog	757 (88.77)	228 (32.28)	943 (97.78)	872 (115.99)	421 (45.43)	159 (9.19)	3,380 (389.47)
Fen	5,326 (740.24)	2,231 (244.95)	4,864 (591.84)	6,041 (701.99)	2024 (208.85)	827 (58.55)	21,313 (2,546.44)
Marsh	1,563 (62.46)	1,323 (44.26)	1,200 (57.17)	587 (43.30)	178 (8.76)	190 (9.10)	5,041 (225.07)
Swamp	4,724 (356.27)	2,320 (169.55)	4,605 (322.04)	5,021 (381.43)	1580 (116.57)	757 (38.57)	19,007 (1,384.45)
Shallow Water	649 (20.15)	358 (8.02)	654 (17.77)	521 (14.82)	294 (5.27)	166 (5.44)	2,642 (71.48)
Deep Water	393 (168.82)	164 (57.84)	395 (107.63)	432 (146.36)	191 (80.26)	20 (11.82)	1,595 (572.76)
Forest	26,587 (2,529.77)	14,066 (1,233.99)	20,390 (1,805.04)	17,805 (1,784.61)	6,536 (632.20)	3,706 (295.70)	89,090 (8,281.34)
Grassland/ Shrubland	7,676 (1,781.80)	2,731 (480.27)	2,103 (321.90)	2,156 (267.49)	803 (78.09)	291 (27.85)	15,760 (2,957.44)
Cropland	18,721 (6,416.17)	19,181 (6,374.03)	47,302 (5,850.99)	48,748 (5,916.98)	16,804 (5,793.80)	15,684 (5,848.69)	166,440 (36,200.69)
Barren	47 (72.67)	89 (68.58)	10 (29.33)	25 (20.12)	0 (0)	0 (0)	171 (190.70)
Total	66,443 (12,237.16)	42,691 (8,713.81)	82,466 (9,201.54)	82,208 (9,393.12)	28,831 (6,969.27)	21,800 (6,304.96)	32,4439 (52,819.89)

TABLE II
MERGING ALL CLASSES INTO DIFFERENT CATEGORIES TO BE USED IN THE CHANGE ANALYSIS

Category-1	Category-2	Category-3
Bog	Vegetated Wetland	Wetland
Fen		
Marsh		
Swamp		
Shallow water	Shallow Water	Non-wetland
Deep Water	Deep Water	
Forest	Vegetated Non-wetland	
Grassland/Shrubland		
Cropland	Anthropogenic	
Barren		

acquired from 1984 to 2020. As outlined in Table III, the images from every three years (1984–1998) or every two years (1999–2020) were combined to produce cloud-free mosaic images from all of Alberta. This was because the study area is covered by clouds and snow most of the times, and creating cloud-free images with less time intervals (*T*), such as annual images, were not possible. In total, 16-time intervals were considered and, thus, 16 wetland maps were produced to analyze changes over the past four decades.

III. METHOD

The proposed methodology includes three main steps. Initially, all the available reference samples (see Table I) were analyzed to select the spectrally unchanged samples to be used in the classifications of the years when no reference sample existed (Section III-A). Then, the selected samples were applied to the proposed classification algorithm to produce wetland maps at different time intervals (Section III-B). Finally, a CD algorithm was applied to assess wetland trends over the past four decades (Section III-C).

TABLE III
LANDSAT IMAGES USED AT DIFFERENT TIME INTERVALS (I.E., TWO OR THREE YEARS) TO PRODUCE 16 WETLAND MAPS

Time Interval Number	Time Interval Range	Landsat-5	Landsat-7	Landsat-8	Number of Images
T1	1984-1986	×			1,556
T2	1987-1989	×			1,771
T3	1990-1992	×			1,846
T4	1993-1995	×			1,917
T5	1996-1998	×			1,935
T6	1999-2000	×	×		1,938
T7	2001-2002	×	×		2,644
T8	2003-2004	×			1,362
T9	2005-2006	×			1,419
T10	2007-2008	×			1,271
T11	2009-2010	×			1,290
T12	2011-2012		×		1,998
T13	2013-2014			×	2,994
T14	2015-2016			×	3,081
T15	2017-2018			×	3,140
T16	2019-2020			×	3,059

The time interval which is bold was used as the reference time interval for change analysis.

A. Unchanged Reference Samples Selection

As clear from Table I, reference data were available from only six years out of the total 37 years. However, to conduct supervised classifications over all 16 intervals provided in Table III, reference samples were required for each interval. Therefore, references samples for the intervals with no samples had to be generated using other methods. For this purpose, a method called the Continuous Change Detection and Classification (CCDC, [43]) was used. The general procedure is illustrated in Fig. 2 and is explained below. In summary, CCDC analyses all the reference samples and only the samples whose spectral responses have not changed during the past four decades. These samples were called unchanged reference samples.

The first step for applying CCDC was masking cloud, cloud shadow, and snow/ice from the Landsat images to use only clear

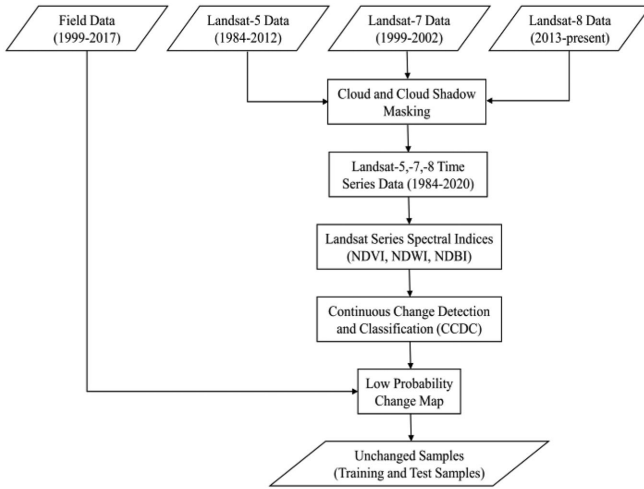


Fig. 2. Continuous CCDC algorithm for selecting spectrally unchanged reference samples over the past four decades from the study area (NDVI, NDWI, NDBI).

pixels. This was performed using the quality band of Landsat (i.e., *Bitmask for pixel_qa*) within GEE. The attributes of this band were generated using the C Function of Mask (CFMASK) algorithm [47]. In this band, the undesired pixels (e.g., cloud and snow) are flagged using either the class name or with the word *unused* depending on the Landsat generation [48]. In this study, Landsat bands were initially converted to three spectral indices of the Normalized Difference Vegetation Index [NDVI, (1)], Normalized Difference Water Index [NDWI, (2)], and Normalized Difference Build-up Index [NDBI, (3)]. These indices were then used to select the unchanged samples. These three indices have proved to have a high potential for wetland mapping and change analysis in many wetland studies. Moreover, they contain all important spectral bands of Landsat satellites [e.g., green, red, near infrared (NIR), and shortwave infrared (SWIR)]. Consequently, the sole use of them was satisfactory for selecting unchanged reference samples and significantly reduced the processing time.

$$\text{NDVI} = \frac{\text{NIR} - \text{RED}}{\text{NIR} + \text{RED}} \quad (1)$$

$$\text{NDWI} = \frac{\text{Green} - \text{NIR}}{\text{Green} + \text{NIR}} \quad (2)$$

$$\text{NDBI} = \frac{\text{SWIR} - \text{NIR}}{\text{SWIR} + \text{NIR}} \quad (3)$$

A model (4) was developed to perform CCDC and, in fact, to define unchanged reference samples

$$F(i, x) = a_{0,i} + a_{1,i} \cos\left(\frac{2\pi}{t}x\right) + b_{1,i} \sin\left(\frac{2\pi}{t}x\right) + c_{1,i}x \quad (4)$$

where i , x , and t , respectively, indicate the spectral index, Julian date, and the number of days per year (i.e., 365.25 days); $a_{0,i}$ stands for the overall value of the spectral index i of a Landsat image; $a_{1,i}$ and $b_{1,i}$ specify the intra-annual change; and $c_{1,i}$

show the inter-annual change. Based on the available reference samples for any specific time interval, the coefficients of (4) were determined. Then, every new sample was inserted into this equation to estimate the model value and model residual by comparing the observed and model values of the samples. In this study, the threshold value was set to 20%, meaning that if the residuals exceeded this threshold value, then an abrupt (or inter-annual) change occurred over that sample and, therefore, that reference sample could not be used in the classification of another time. At the end of this process, only samples that had stable spectral responses remained and, thus, could be applied to classify wetlands over all 16 intervals. Finally, these unchanged reference samples were randomly divided into two groups of training (50%) and test (50%) samples. The training and test samples were used for training the machine learning algorithm and assessing the accuracy of the produced wetland maps, respectively.

B. Classification

After generating unchanged reference samples using the method described in the previous section, wetland maps were produced for each time interval using the method presented in Fig. 3. The first step was masking cloud, cloud shadow, and snow/ice pixels from all images. Then, these images were divided into two groups based on the season in which they were acquired: 1) the months of April, May, June, and July, which was called the *Spring-Summer* time, and 2) the months of August, September, and October, which was called the *Summer-Fall* time. Subsequently, all the images in each group were down-sampled to a single mosaic image by taking the mean over the entire time series images (i.e., the *Spring-Summer* and *Summer-Fall* mosaic images).

In this study, considering the computation efficiency of the proposed classification method, 10 features were extracted from each mosaic image and were used in the classification [49]. These features (layers) were the seven main spectral bands of Landsat images (i.e., blue, green, red, NIR, two SWIR, and thermal infrared TIR bands) and three spectral indices of the NDVI, NDWI, and NDBI.

It has been widely reported that object-based classification techniques produce better results compared to pixel-based methods [1], [10], [50], [51]. Additionally, wetland classes are large heterogeneous landcover types that require an object-based analysis [52]. Therefore, the mosaic images were ingested into the simple noniterative clustering (SNIC) algorithm, available in GEE, to be segmented. In the SNIC method, initially, a number of seeds were evenly distributed throughout the image to partition it into several number of superpixels. Then, a priority queue was applied to select the next pixel to be assigned to a cluster based on the distance of the pixel from the segment centroid. After adding each new pixel to a segment, a new centroid was computed. This process continued until centroid convergence [53].

The final segmented mosaic image with 20 layers (i.e., 10 layers from each of the *Spring-Summer* and *Summer-Fall* mosaic images) was ingested into a supervised random forest (RF) classifier. RF has proved to be an effective classifier for image classification, especially for wetland mapping [1], [10], [54].

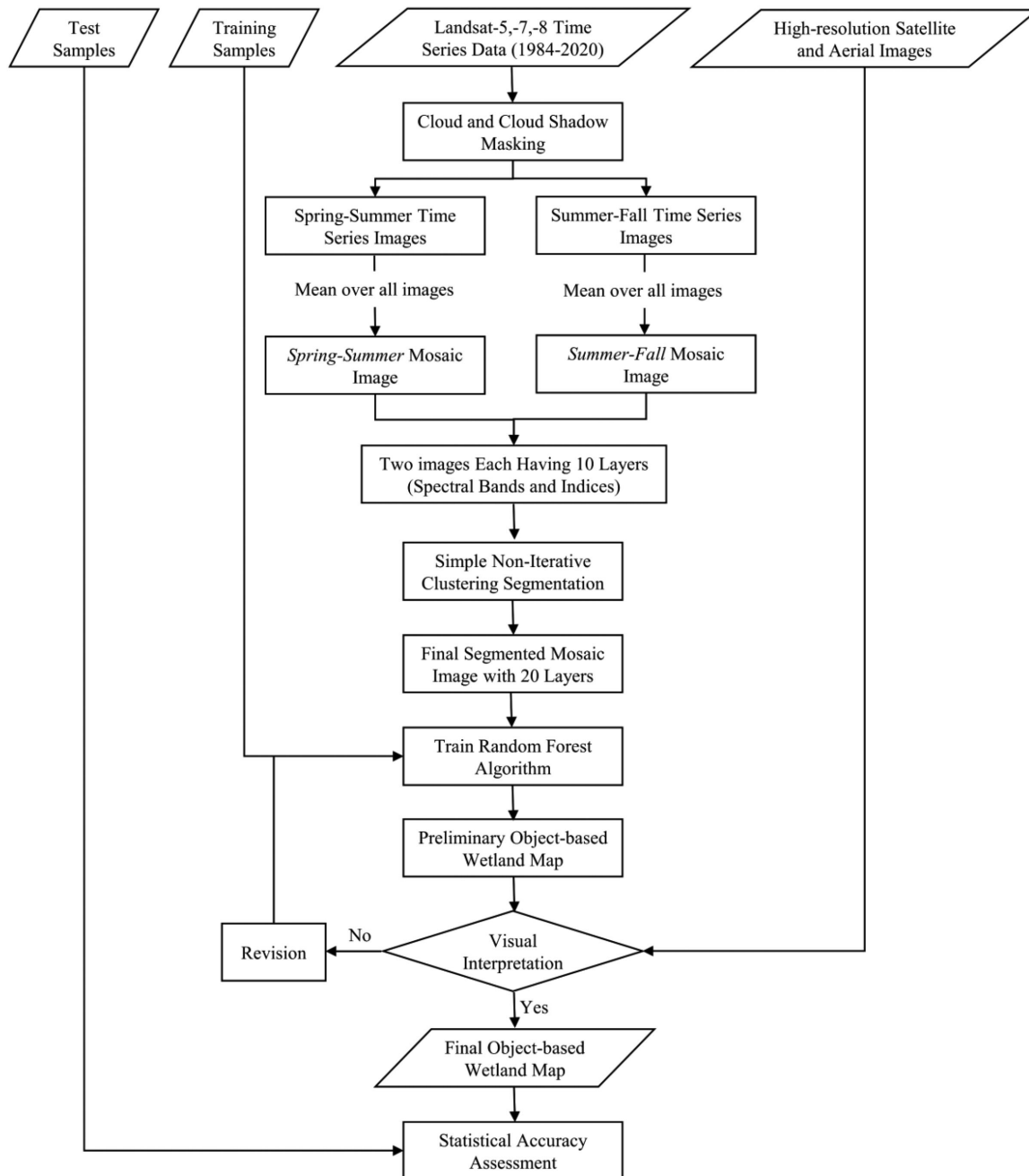


Fig. 3. Classification method to produce wetland maps.

RF contains a set of decision trees that divide the input pixels into mutually exclusive groups until each node represents one of the final classes. RF has a number of tuning parameters that should be selected based on the available samples and the objectives of classification [54]. In this work, these parameters were selected after several trials and errors and based on the results of previous wetland mapping studies within GEE [55], [56].

After the classification was conducted, it was first visually assessed based on the available high-resolution maps and images (e.g., ArcGIS base maps). If the results were not satisfactory, the classification parameters and/or the training samples were revised, and the classification was repeated until visually accurate results were obtained. For the statistical accuracy assessment,

the maps were compared with the test data (i.e., 50% of the field samples), and the result of this comparison was presented in the form of a confusion matrix. To this end, several indices, including overall accuracy (OA), Kappa coefficient (KC), producer accuracy (PA), user accuracy (UA), omission error (OE), and commission error (CE), were extracted from the confusion matrix and reported.

C. Change Detection

After producing all the 16 wetland maps, change analysis was conducted using the methods provided in the two following subsections. To implement the proposed CD method, it was

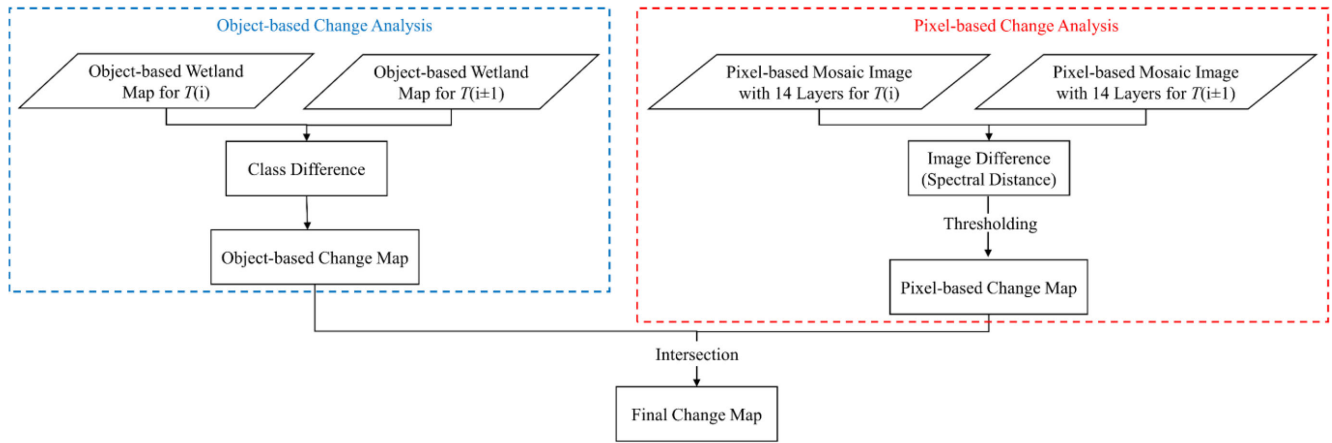


Fig. 4. Method for wetland CD between two time intervals. T indicates the time interval (see Table III).

important to first detect the changes between every two time intervals (Section III-C1) in order to detect the overall changes over the past four decades (Section III-C2). Moreover, it was required to select one of the time intervals/maps as a reference interval/map. In this study, the map produced for 2007–2008 (T_{10} in Table III) was selected as the reference map due to the relatively higher quality of this map and availability of more reference samples from this interval compared to others (see Table I). It should be noted that changing this reference interval does not considerably affect the change analysis, and this is in fact, only a start point for the CD algorithm.

1) *CD Between Two Time Interval*: Fig. 4 illustrates the proposed method for the CD between two-time intervals using the seven spectral bands of the *Spring-Summer* and *Summer-Fall* mosaic images. To this end, two different CD methods of class differencing and image differencing were combined to produce the final change map. A combination of two methods resulted in more accurate change results compared to using only one of them. Furthermore, using the pixel-based and object-based CD methods reduced the overestimation in the changed areas and noises, respectively.

The object-based change analysis was conducted by differencing two object-based wetland maps. On the other hand, the pixel-based change analysis was conducted using the spectral distance between the mosaic images of two-time intervals based on the spectral angle mapper distance. To this end, the per-pixel distance between each pair of mosaiced images was calculated using “*ee.Image.spectralDistance*” function in GEE. Later, the threshold value was set to determine the unchanged samples between each time interval. In this study, a threshold value of 70% was selected after several trial and errors to make sure that there were enough unchanged reference samples to train the algorithms and validate the results. This threshold value means that if the difference between the spectral responses of pixels at two different time intervals were more than 70%, they were selected as the changed pixels. Finally, the intersection of the pixel- and object-based change maps was considered as the final change map. It should be noted that the final change map was object-based.

2) *CD Through All Time Intervals*: Since the main objective was analyzing the changes over the entire 16-time intervals,

a method (see Fig. 5) was also proposed to obtain the overall changes over the past four decades. If it is assumed that the reference time interval (i.e., T_{10} in this study) is one of the two maps for change analysis in Fig. 4, the other map (e.g., T_{11}) can be updated after producing the final change map. In fact, the class labels of the changed objects in the second map (T_{11}) can be updated based on the labels of the reference map. In this study, considering this approach, all the 15 wetland maps (other than the reference map) were hierarchically updated using the method illustrated in Fig. 5. Finally, the difference between the updated wetland maps of T_1 and T_{16} was the overall changes that occurred over the past four decades.

IV. RESULTS AND DISCUSSION

A. Classification

1) *Classified Maps*: All the 16 wetland maps were produced using the method discussed in Sections III-A and III-B. One of the maps produced for the reference time interval (2007–2008) is illustrated as an example in Fig. 6. Based on the visual accuracy assessment, the maps were quite accurate. For example, large water bodies were accurately classified as Deep Water, while the small areas around them were either mapped as Shallow Water or Marsh. Moreover, the southwest part of the map, where the Rocky Mountains are located, were correctly classified as Barren. Likewise, the croplands were delineated accurately. Overall, based on the visual accuracy assessments, it was observed that all maps had acceptable accuracies.

2) *Accuracy Levels*: Fig. 7 demonstrates the OAs and KCs for all 16 maps. As can be seen, all the OAs were around 88% which were considerably high for mapping an area as large as a province with only optical Landsat data. Moreover, KCs were never lower than 86%, indicating a good agreement between the produced maps and reference data. The maximum accuracies were obtained for the time intervals of 2009–2010 and 2007–2008 (reference map), and the minimum accuracies corresponded to the time intervals of 2015–2016 and 1999–2000. However, the variation of the accuracies was rather consistent among different years, such that the difference between the maximum and minimum accuracies was less than 1%. This fact

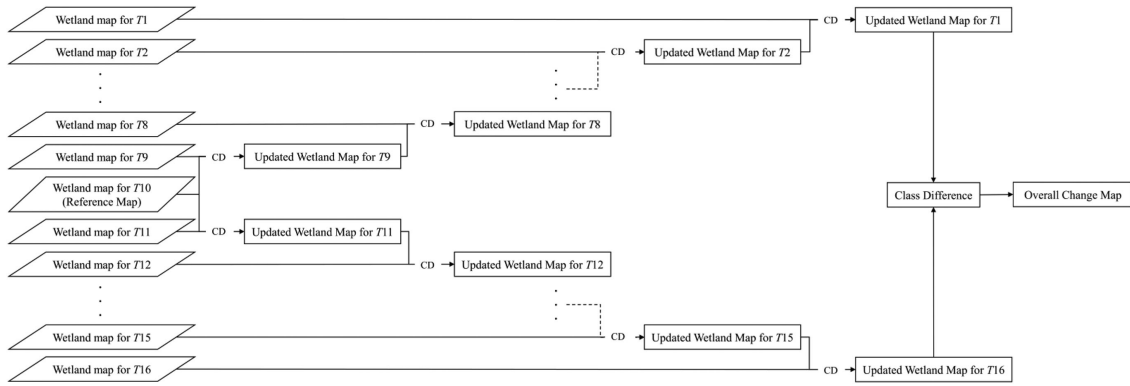


Fig. 5. Method for wetland CD over the entire four decades. *T* indicates the time interval (see Table III) and CD is the method proposed in Fig. 4.

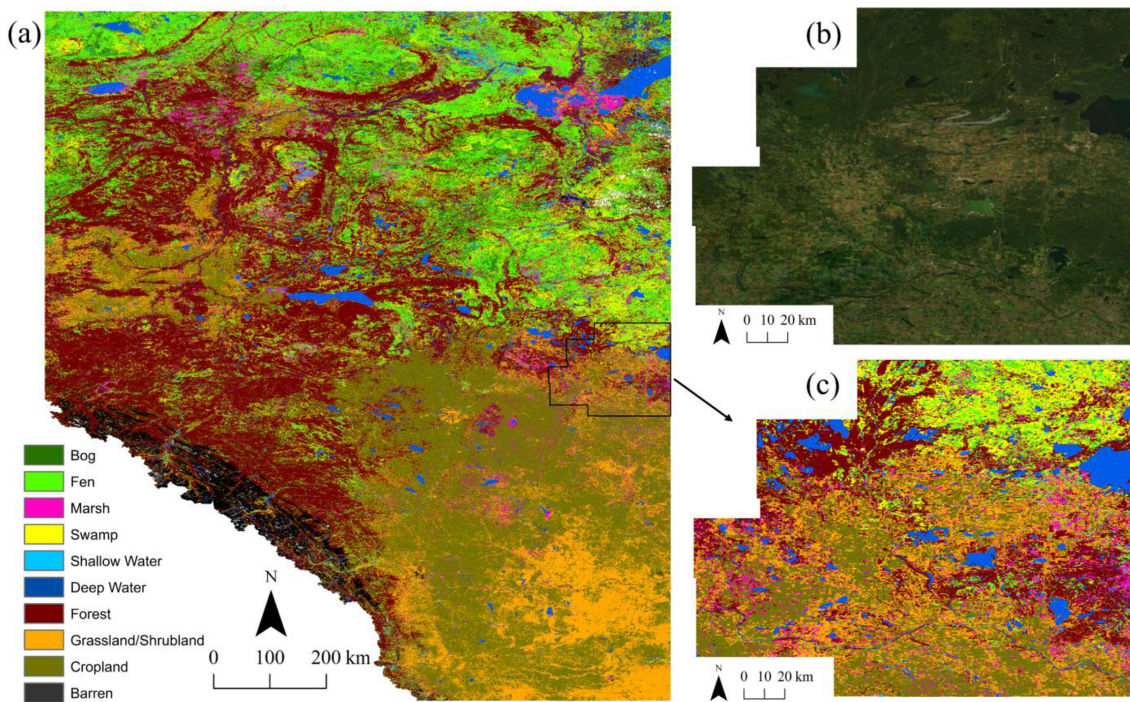


Fig. 6. (a) Produced wetland map for the reference time interval (i.e., 2007–2008) along with (b) high-resolution image and (c) zoomed wetland map from the Cold Lake oil sand.

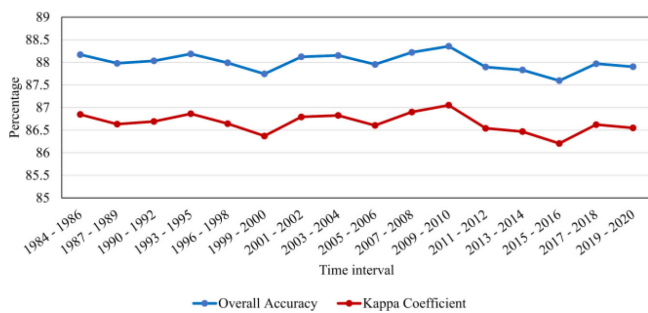


Fig. 7. Overall classification accuracies and KCs for the wetland classified maps in different time intervals.

proved the robustness of the proposed GEE method for wetland classification using Landsat imagery.

Fig. 8 shows the PAs and UAs for all time intervals. The PAs and UAs for all classes in different time intervals except for the UAs of the Swamp class were more than 80%, indicating the high potential of the developed method to discriminate different wetland and nonwetland classes using Landsat data. As expected, the Barren and Deep Water classes had the highest PAs and UAs, ranging from 96% to 100%. The reason can be attributed to the spectral signatures of these two classes, which are easily distinguishable from the other classes. The PAs of the Shallow Water class and the UAs of the Bog class were also very high (~95%).

The confusions between different classes in the wetland maps were also investigated using the confusion matrices of the classifications. For this purpose, the confusion matrix corresponding to the reference wetland map is provided in Table IV as an example.

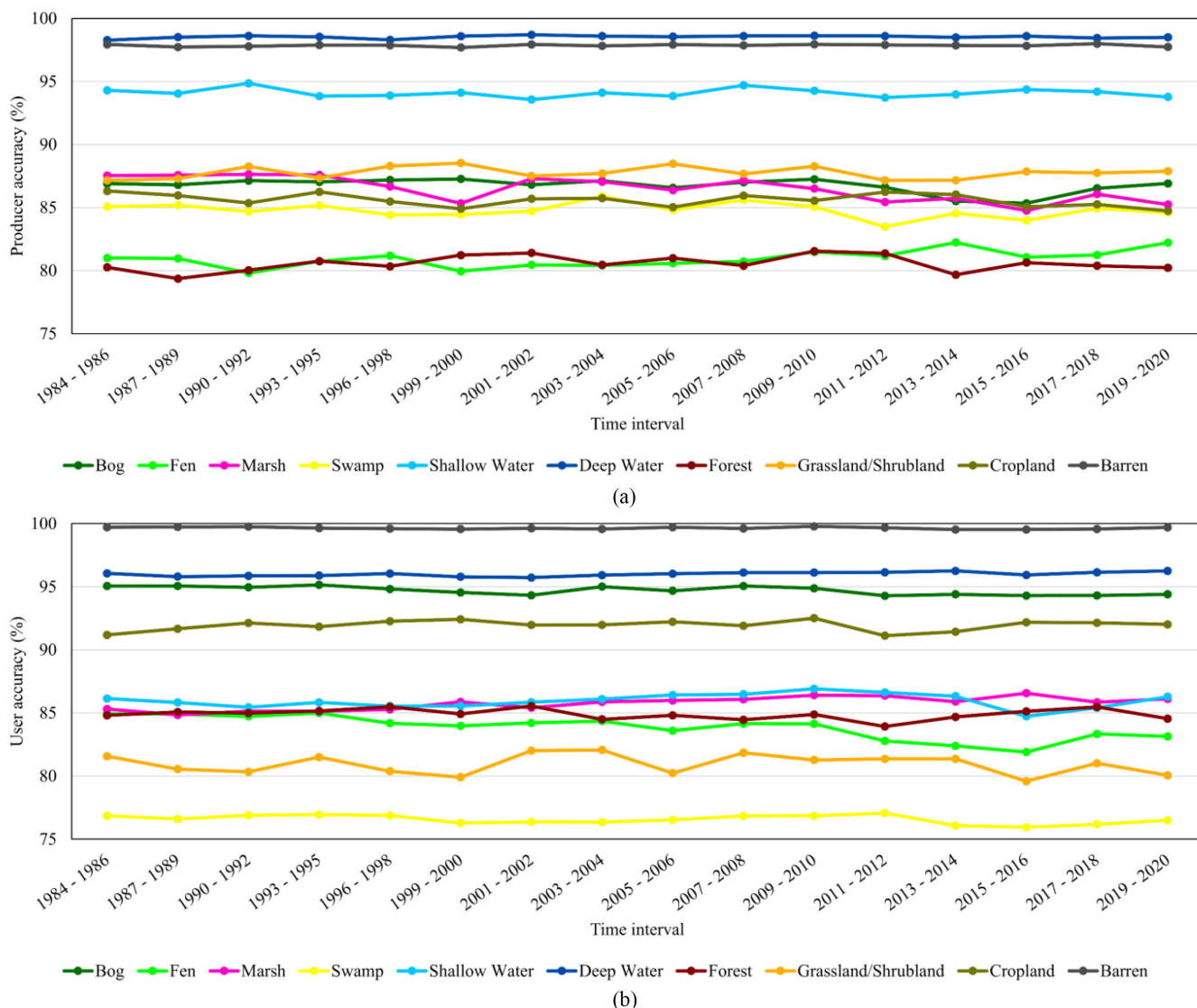


Fig. 8. Producer and user accuracies for various classes in different time intervals.

TABLE IV
CONFUSION MATRIX OF THE REFERENCE WETLAND MAP (TIME INTERVAL OF 2007–2008) BASED ON THE NUMBER OF PIXELS

	Reference Data										Total
	Barren	Bog	Cropland	Deep Water	Fen	Forest	Grassland/Shrubland	Marsh	Shallow Water	Swamp	
Barren	94,155	6	13	12	87	135	63	19	13	11	94,514
Bog	14	95,199	3	23	2,008	1,000	11	263	67	1,556	100,144
Cropland	11	10	92,252	5	82	218	7,022	717	48	7	100,372
Deep Water	100	246	119	93,943	650	802	117	819	527	411	97,734
Fen	35	6,395	65	133	83,926	2,892	144	1,379	418	4,346	99,733
Forest	374	1,538	778	153	4,584	84,874	1,468	1,773	441	4,501	100,484
Grassland/Shrubland	1,414	166	10,273	78	1,371	2,757	82,035	1,582	224	327	100,227
Marsh	48	662	3,263	441	2,118	3,458	1,750	85,813	1,294	843	99,690
Shallow Water	44	470	423	334	1,645	2,522	512	3,473	66,019	896	76,338
Swamp	15	4,712	139	148	7,484	6,907	446	2,624	664	76,763	99,902
Total	96,210	109,404	107,328	95,270	103,955	105,565	93,568	98,462	69,715	89,661	969,138

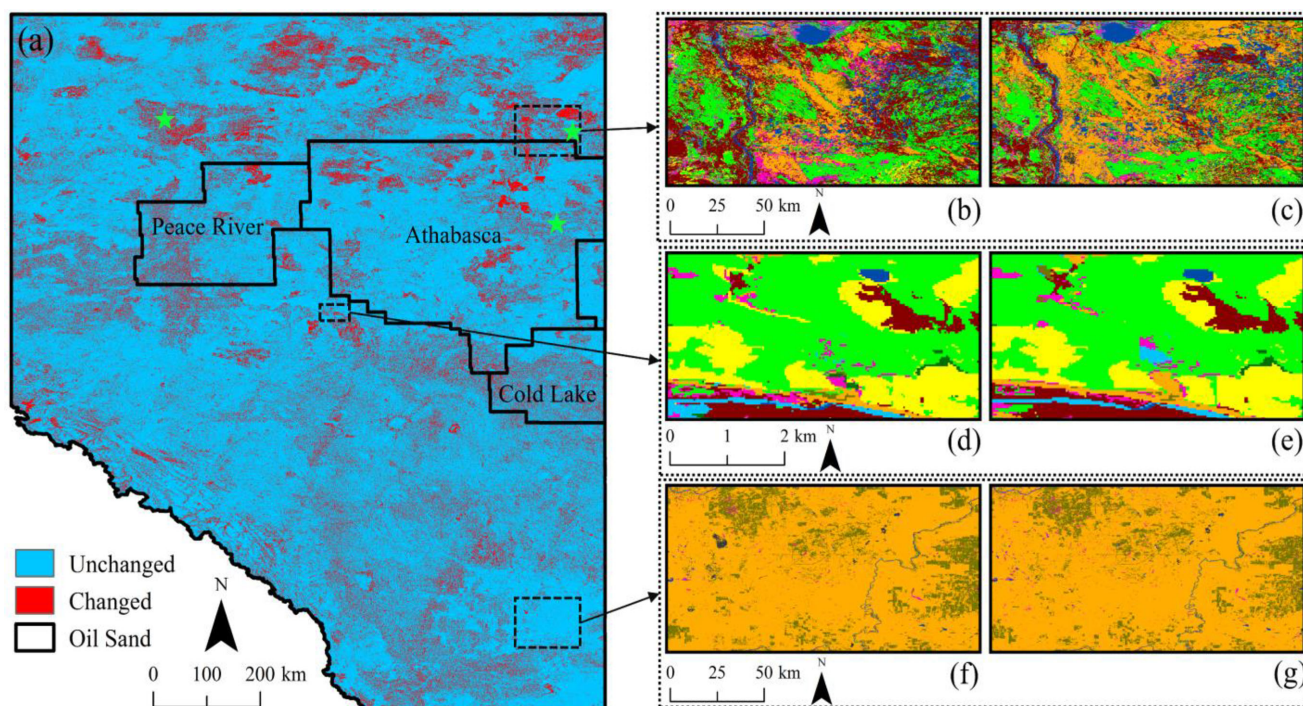


Fig. 9. (a) Binary changed/unchanged map of Alberta over the past four decades. Zoomed maps of the (b), (d) first and (c), (e) last time intervals as examples of the major and minor rates of land cover changes, respectively (see Fig. 6 for the legend of the classification). Green stars show the locations of three wildfire events for further investigations.

As expected, the highest confusions occurred between the wetland classes. This is because the wetland classes share many ecological characteristics, which causes their spectral signatures to be similar. In this regard, the confusion between the Bog and Fen classes was more significant, which is rooted in the fact that Bog and Fen are the most similar wetland classes. For example, 6395 pixels out of the 109404 pixels of the Bog class were wrongly classified as Fen. These two classes were also mixed with the Swamp class. For instance, 4712 and 7484 samples of the Bog and Fen classes were incorrectly classified as the Swamp class, respectively. This was, in fact, the main reason for the low UA of the Swamp class. Furthermore, relatively high confusions were also observed between Marsh and other wetland classes. In fact, the condition of emergent Marsh was closely related to local weather patterns, which can make these areas to be flooded at the time of imaging, such that the classifier was unable to discriminate Marsh from Shallow Water. On the other hand, meadow Marsh can also bring difficulties for the classifier to separate these areas from Bog and Fen [57]. Finally, it was observed that the confusion between wetland classes is less significant in the case of Shallow Water as this class is less similar to the other wetland classes.

Some wetland classes were also mixed with nonwetland classes, especially Forest, Grassland/Shrubland, and Cropland classes. In this regard, the main confusion was related to the confusion between the Swamp and Forest classes. This was because these two classes are mainly treed classes, the discrimination of which is challenging using only optical satellite data. For example, 4501 out of 89661 samples of the Swamp class were misclassified as the Forest class. Likewise, 6907 out of 105565 samples of the Forest class were incorrectly classified

as Swamp. This fact was another reason for the low UA of the Swamp class. Moreover, the Marsh, Shallow Water, and Fen classes had a slight confusion with the Deep Water class. This might be because wetlands, as highly dynamic environments, are sometimes flooded, and can therefore be easily confused with the Deep Water class.

Among the nonwetland classes, Barren and Deep Water had the least confusion with other classes. The highest confusions were observed between the Cropland and Grassland/Shrubland classes, as well as between the Forest with other vegetated nonwetland (VN) classes. For example, 9.57% of the Cropland samples were misclassified as Grassland/Shrubland.

B. Change Analysis

After producing 16 wetland maps, several CD analyses were performed to examine changes from different perspectives. Since the achieved OAs of the maps were high, the produced CD maps also had high reliability for further investigations. However, it is worth noting that although all the wetland maps obtained high OAs, the inherent misclassifications and errors (e.g., see Section IV-A-2) would definitely propagate into the results of CD analyses steps, causing different uncertainties. The CD analyses are explained through spatial and statistical investigations in the following subsections.

1) *Overall Change*: The first change analysis (see Fig. 9) was a binary changed/unchanged map over the past four decades, presenting any land cover change between the Category-1 classes (see Table II). The results showed that approximately 18.25% of Alberta (120919 km²) was subjected to changes, while the remaining 81.75% (541734 km²) were unchanged. Visually, the

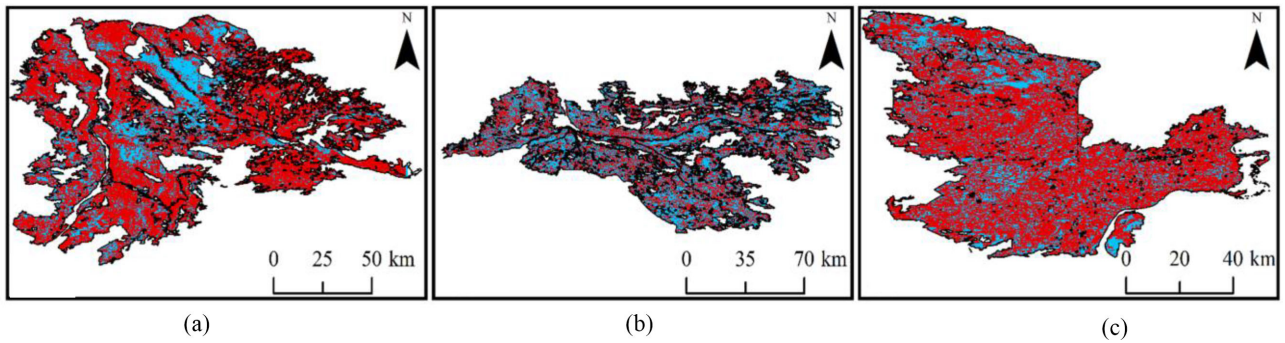


Fig. 10. Changed/unchanged maps over three fire events of (a) Richardson fire, (b) Horse River fire, and (c) Chuckegg Creek fire (see Fig. 9 for the legend). The central location of each fire event is determined by green stars in Fig. 9.

spatial patterns of changed/unchanged areas do not have specific regularity across the study area. However, several parts, such as the northern and north-eastern regions, can be mentioned as the hotspots, in which more intense changes occurred. For instance, Fig. 9(b) and (c) shows the maps of the first and last intervals over a zoomed area, which includes severe changes between different land cover classes, especially Fen degradation to Grassland/Shrubland. Further investigations revealed that some of the changes in this area are linked with the Richardson wildfire event in 2011, causing peatland (i.e., Bog and Fen) losses and in the last time interval become shrubby and, thus, were classified as Grassland/Shrubland. Likewise, considerable changes were observed in the oil sands regions [black boundaries in Fig. 9(a)], which could probably be due to the oil exploration activities and infrastructure development [58]. However, other climatic alterations in the last four decades, intra-annual land cover variability, and catastrophic events can be considered as causes of higher land cover changes, which requires further investigations. For example, based on the changed/unchanged map illustrated in Fig. 9, the Cold Lake region experienced nearly 23.32% change, which was 5.07% higher than Alberta's overall change. Additionally, Fig. 9(d) and (e) presents a zoomed area, in which a Fen area was changed into Shallow Water. Further investigations using satellite images revealed the impact of the anthropogenic (AN) activities of road construction, leading to hydrological alteration of wetland regions. This result was also in accordance with a previous study by Willier [59], which conducted a field survey over this region. On the other hand, the southwest and southeast regions [e.g., Fig. 9(d) and (e)] were among the most unchanged parts of Alberta between 1984 and 2020. This is likely due to the relative amounts of wetlands in this area and the uniform landcover types (conifer forest/barren for the Rocky Mountains and grassland/agriculture for the south-east).

Additionally, the applicability of the proposed CD method was also examined by analyzing its capability to capture intense changes that occurred from wildfire events. In this regard, three different wildfire events, including Richardson, Horse River, and Chuckegg Creek fires, which happened in 2011, 2016, and 2019, respectively, were analyzed [60]. To this end, the classification maps of the relevant (i.e., T associated with the wildfire event) and previous intervals were used to generate the changed/unchanged maps of each event (see Fig. 10). Fig. 10(a) shows the changed/unchanged map over the catastrophic Richardson wildfire event that resulted in a vast area

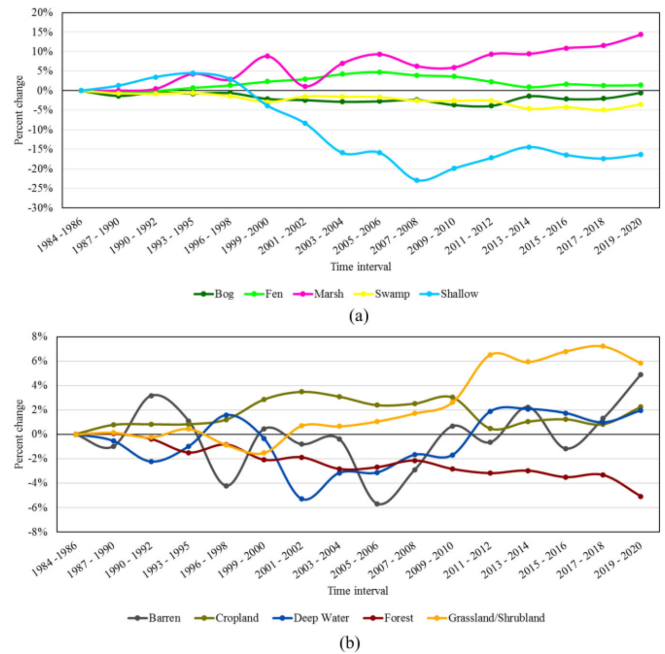


Fig. 11. Change trends for the (a) wetland classes and (b) non-wetland classes in Alberta from 1984 and 2020. The rates indicate the percent of change in area relative to the first-time interval.

being consumed by fire. Likewise, the proposed method successfully delineated the changed areas related to the Horse River wildfire event [see Fig. 10(b)], which resulted in peatland burn losses [61]. Additionally, Fig. 10(c) illustrates the immense changes that occurred after the Chuckegg Creek wildfire event, in which a vast spatial extent of forests burned.

2) *Change Trend Analysis:* The change trends between 1984 and 2020 for wetland and nonwetland classes are illustrated in Figs. 11 and 12. Regarding wetland classes, the changes for the Fen, Bog, and Swamp classes were relatively stable [see Fig. 11(a)]. Moreover, Fig. 11(a) shows that Shallow Water dramatically declined from 1984 to 2007 and, then, took an upward trend and compensated its decrease by about 6.57%, reaching -16.33% in 2020. This amount of decrease was unexpected and might be due to the misclassification with the Deep Water class in the produced maps. In contrast, Marsh had an overall upward trend almost in all time intervals, except for a notable reduction in 2001, leading to a final overall growth of 14.36%.

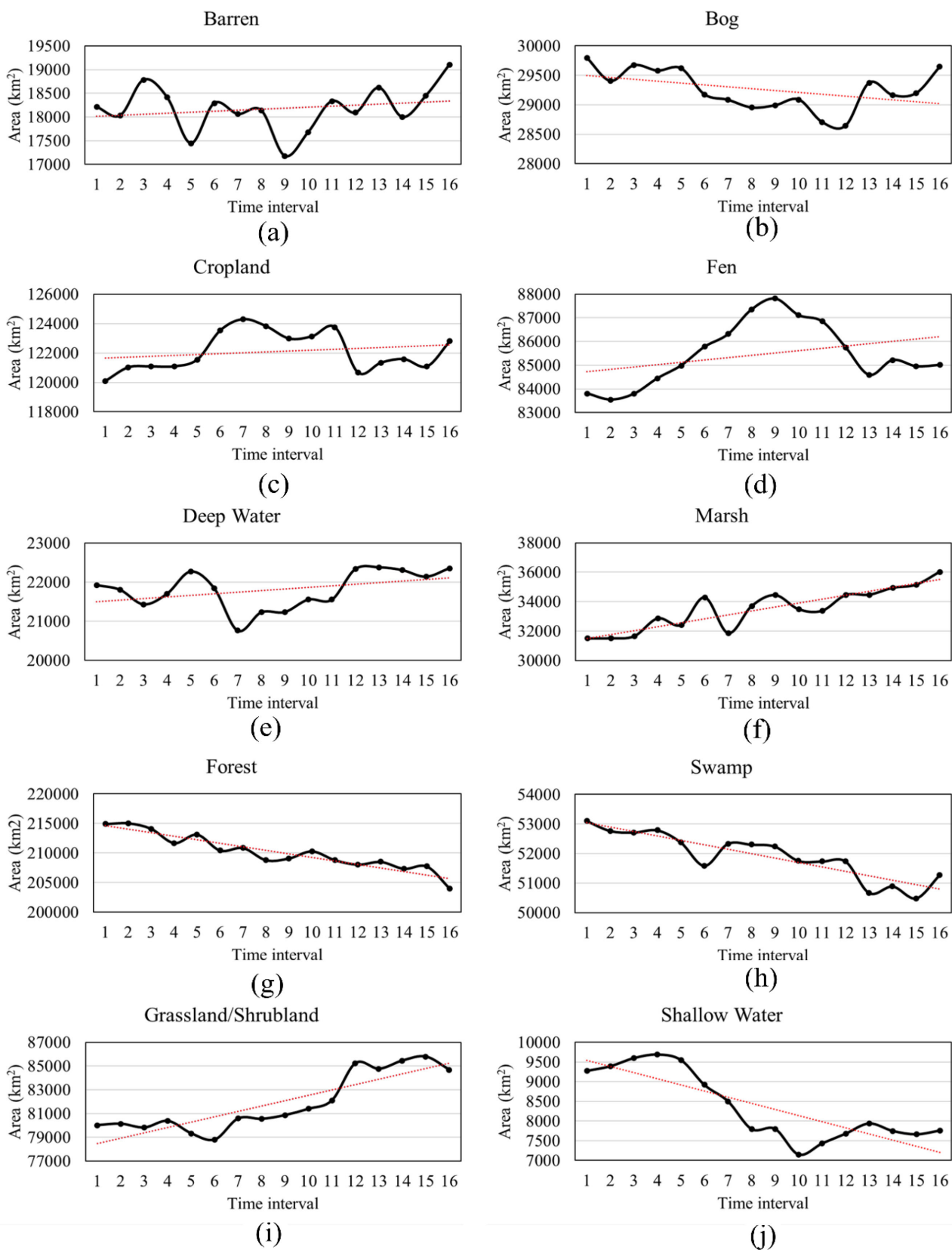


Fig. 12. Variation of the area of each class over the past four decades (see Table III for the corresponding years of each time interval).

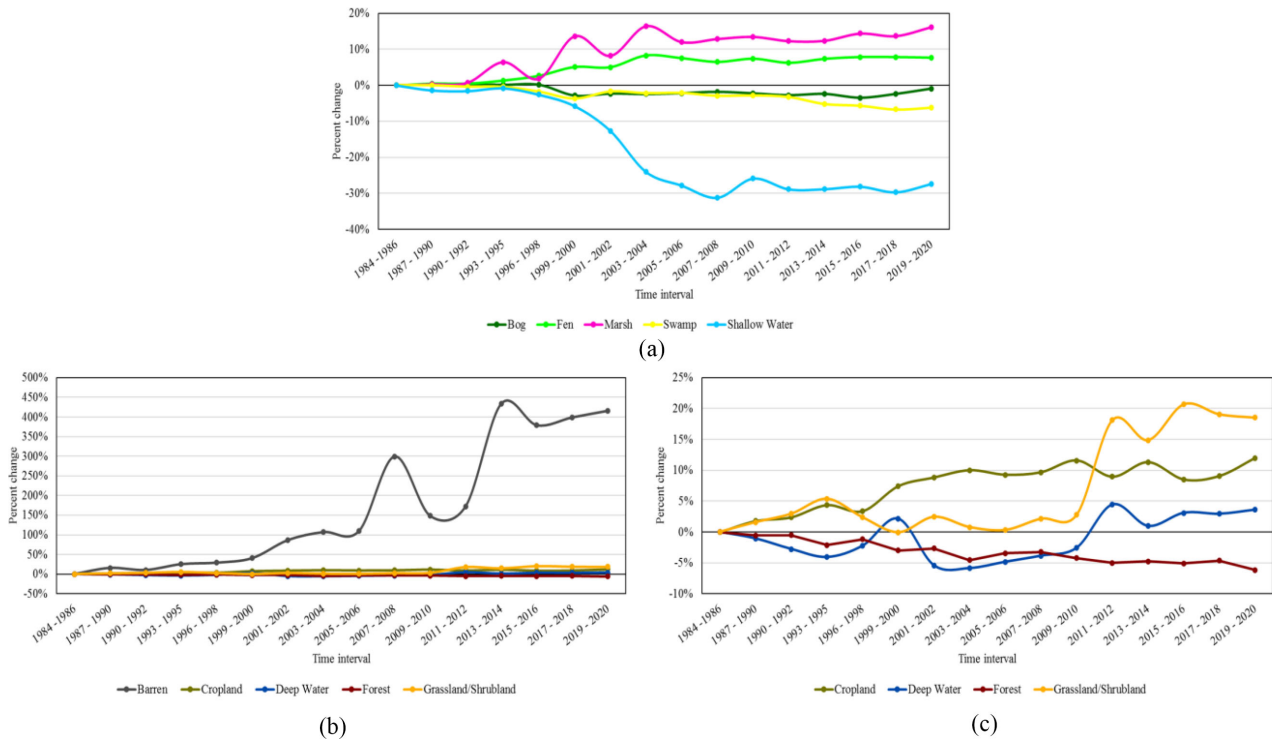


Fig. 13. Rate of changes for the (a) wetland classes and (b) and (c) nonwetland classes in Alberta from 1984 to 2020 over three oil sand regions (i.e., Athabasca, Cold Lake, Peace River). The rates indicate the percent of change in area relative to the first time interval.

Regarding nonwetland classes, they experienced a higher rate of oscillations compared to wetland classes. For instance, the fluctuations for the Barren and Deep Water classes were considerable [see Fig. 11(b)]. Although Barren and Deep Water were respectively decreased by about 6% until 2005 and 2001, their significant increase in the subsequent years resulted in a total gain of approximately 4.90% and 1.96%. Human-induced activities, such as urban expansion, mining, and infrastructure development, as well as climatic alterations and natural events, could be the main reasons for Barren growth in Alberta, though more investigations are required for a firm conclusion. Additionally, Forest had a more stable downward trend and almost declined in nearly all-time intervals and took about 5.08% loss between 1984 and 2020 (10927 km²). Although AN activities (i.e., agricultural expansion and oil/gas explorations) can be regarded as deforestation reasons, this considerable amount of loss was mainly due to forest fires and wildfires in Alberta. In particular, based on the National Forestry Database on the Canadian Council of Forest Ministers, over 38000 forest fires were recorded between 1990 and 2019, which resulted in a substantial forest loss [62]. The trends of the Cropland and Grassland/Shrubland classes were also fluctuating in different years; however, their general rising tendency resulted in nearly 2.25% and 5.84% growth in 2020, respectively.

Furthermore, the area of each class in 16 wetland maps was also analyzed in Fig. 12 to explore further change trends over the last four decades. As is clear, the Forest class had significantly more area than other classes. For instance, on average, 31.72% (210182 km²) of the province is covered by different forest types. In terms of wetland classes, the study area is mostly dominated by Fen (12.90% of the province) with an average area

of about 85459 km². The smallest coverage also belonged to the Shallow Water and Barren classes, which on average, cover only 1.26% (8370 km²) and 2.74% (18177 km²) of Alberta.

Based on Fig. 12, the greatest change was related to the Forest class, the area of which decreased by approximately 1.65% of the total study area (from 214915 km² to 203987 km²). Likewise, the Swamp and Shallow Water classes were respectively declined from 53108 km² and 9277 to 51278 km² and 7761 km², which are accounted for 0.27% and 0.22% of the total study area. On the other hand, the Marsh, Cropland, Grassland/Shrubland, Barren, Deep Water, and Fen had an upward trend with increases of approximately 14.36%, 2.25%, 5.83%, 4.89%, 1.96%, and 1.43%, respectively.

As discussed in Section IV-B-1, oil sands regions were among areas with high changes, in which broad disturbances to ecosystems occurred [58]. Therefore, similar trend analyses were also conducted over the three oil sand regions (see Fig. 13). Comparing Figs. 11 and 13, the nonwetland classes had a higher range of fluctuations, while the range of oscillations for wetland classes was modestly similar. Generally, wetland classes over the oil sands regions experienced similar trends to Alberta as a whole, except for the Shallow Water and Fen classes, in which the amount of changes were different, reaching -27.4% and 7.61%, respectively. Fig. 13(b) and (c) presents considerable changes in nonwetland classes over the three oil sand regions. The most notable change in the area was related to the Barren class, by which its area was increased over 400% by the end of 2020. This significant growth was probably due to multiple wildfires which led to deforestation [63], as well as other possible AN activities, such as mining and oil explorations in these areas. Additionally, the variation in the areas of the Forest class over these regions

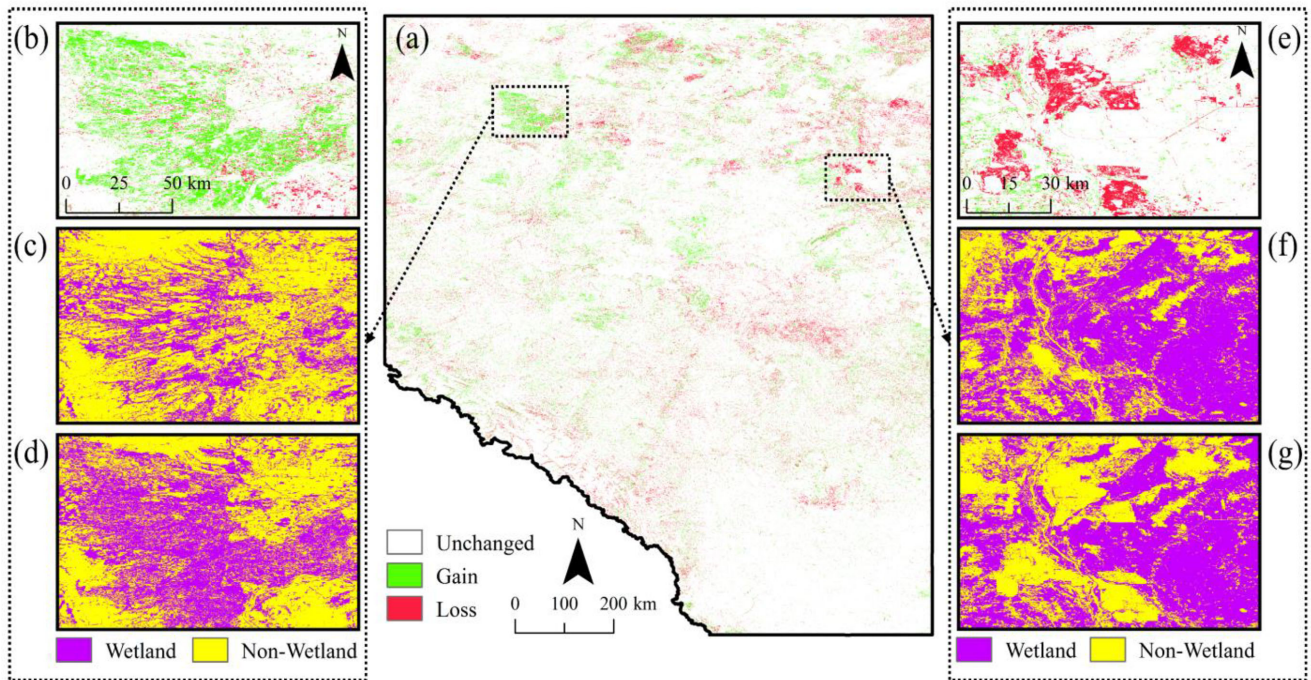


Fig. 14. (a) Spatial pattern of wetland gain and loss over Alberta in the last four decades. (b) Sample area over a dense wetland gain along with the (c) first and (d) last maps of wetland/nonwetland. (e) Sample area with severe wetland loss along with the (f) first and (g) last maps of wetland/nonwetland.

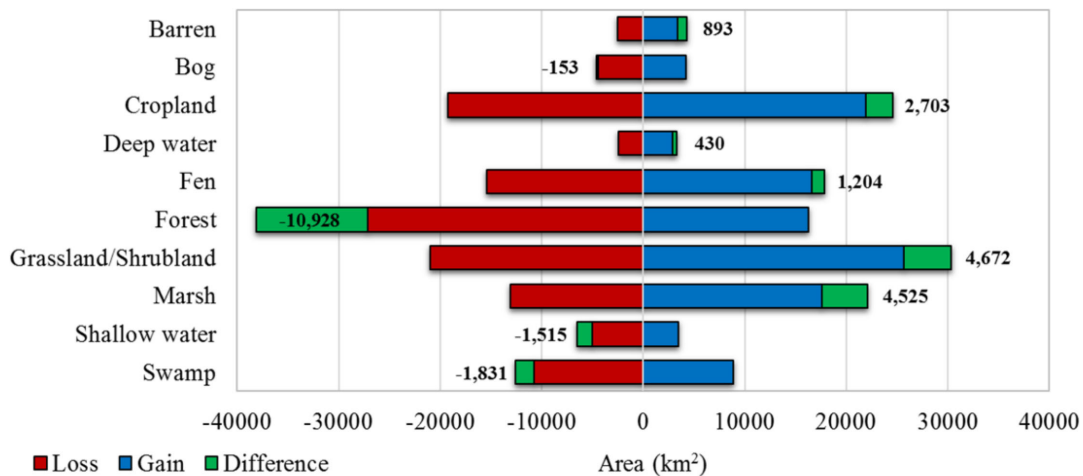


Fig. 15. Loss, gain, and difference between loss and gain values of each class in Alberta over the past four decades. The numbers indicate the difference values.

was higher than all of Alberta by about 1%, reaching -6.16% in 2020.

3) *Gain and Loss*: Several analyses were performed to reveal the gain and loss in wetlands and non-wetlands over the past 40 years (see Figs. 14–16). First, the changed/unchanged map (see Fig. 9) was reclassified into two classes in Fig. 14: 1) areas that the nonwetland classes were converted to the wetland classes (wetland gain); and 2) areas that the wetland classes were converted to the nonwetland classes (wetland loss). As is clear in Fig. 14(a), the northern parts of Alberta were associated with more wetland gain and loss compared with the southern parts. Fig. 14(b)–(d) illustrates a wetland gain area, for which the results suggested that the Forest class was mostly changed to

wetland classes of Swamp and Fen. However, in-depth analyses revealed that this region is associated with the wildfire event of Chuckegg Creek, in which a vast area of forests was consumed by fire, and the burned forest areas were confused with peatlands (e.g., Fen) due to spectral similarity. This similarity is rooted in the fact that the characteristics of the burned forest areas are similar to different moss species (e.g., *Sphagnum Magellanicum*) that grow in boreal wetlands. In contrast, a severe loss, especially for Fen, occurred due to wetland degradation to Barren [see Fig. 14(e)–(g)]. Overall, it was observed that approximately 38.68% of changed areas were related to the land cover transition between wetlands and nonwetlands. In particular, between 1984 and 2020, nearly 24 506 km² of Alberta experienced wetland

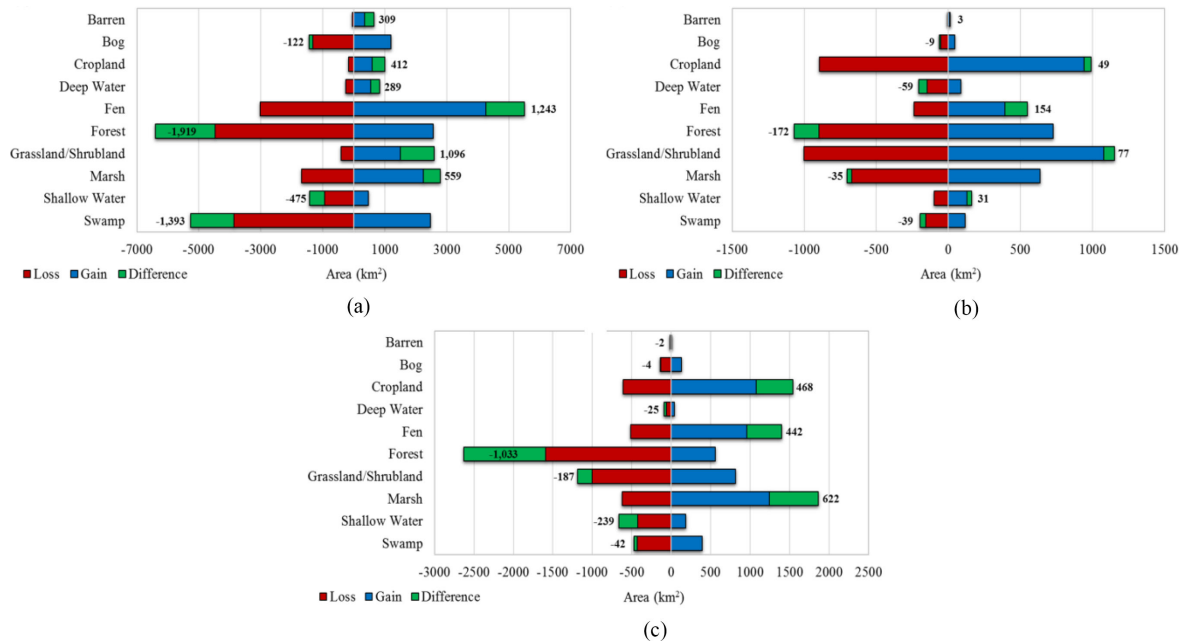


Fig. 16. Loss, gain, and difference between loss and gain values of each class in the (a) Athabasca, (b) Cold Lake, and (c) Peace River oil sands over the past four decades. The numbers indicate the difference values.

gain, whereas around 22271 km² underwent wetland loss. Further investigations showed that this much of wetland gain was mostly associated with the transition of Forest to wetland classes. For example, over 70% of the wetland gain (17217 km²) was related to the Forest transition to the wetland classes of Fen (34.74%), Marsh (27.97%), Swamp (25.07%), Bog (6.28%), and Shallow Water (5.94%). These transitions were generally linked with two reasons: 1) deforestation activities and subsequent abundance that could result in the transition of upland forested areas to wetlands over the past four decades; 2) possible classification errors, especially between Swamp and Forest, due to their spectral similarity when only optical data are used.

Fig. 15 provides a more detailed overview of the gain and loss for each class. The Forest and Grassland/Shrubland classes had the biggest loss. Moreover, Grassland/Shrubland and Cropland were two classes with major gain, respectively. The Fen and Bog classes had the highest and lowest amount of loss among wetland classes with an area of about 15408 km² and 4406 km², respectively. Likewise, Marsh and Bog had the highest and lowest gain of nearly 17580 km² and 4253 km², respectively. The green color in Fig. 15 represents the difference values between gain and loss over the past four decades. Forest, with an approximate area of 10927 km², was subjected to the most severe degradation, while the area of Grassland/Shrubland increased by about 4671 km². In terms of wetland classes, Swamp and Marsh experienced the highest amount of coverage decrease and increase of about 1831 km² and 4524 km², respectively.

Similarly, the statistical gain and loss analysis was performed over the tree oil sand regions (see Fig. 16). Like all of Alberta, these oil sand regions were subjected to higher Forest loss than Forest gain, which resulted in deforestations of about 1919 km², 1033 km², and 172 km² in Athabasca, Peace River, and Cold Lake, respectively. Moreover, a remarkable increase in the areas of the Barren and Cropland classes reflected a greater rate of AN

and human-induced activities. Likewise, the Cropland coverage was increased in the Peace River, which was also associated with deforestation for agricultural expansion. Regarding the change of wetland classes, the area of Fen increased by 1243 km² and 154 km² in Athabasca and Cold Lake, while in Peace River, Marsh had a larger increase of over 600 km². On the other hand, Swamp was the dominant wetland class with declined coverage of about 1474 km² over the oil sand region.

4) *Transition Between Classes:* To further enrich the CD analyses, transitions between each pair of classes were also examined. To this end, the first and last wetland maps were processed to generate the from/to results, which provides the land cover transition between each pair of classes. It should be noted that although the first and last wetland maps achieved acceptable OAs, their possible misclassification are accumulated and affect this step. Fig. 17 shows the Sankey diagram that pictured the transition based on the first and last wetland maps. The quantitative land cover transitions between different classes are also provided as the From/To matrix in Table V. The results showed that Forest was the dominant land cover type in Alberta, followed by Cropland with average areas of about 209450 km² and 121448 km², respectively. Regarding wetland classes, Fen was the dominant class in Alberta with areas of nearly 83807 km² and 85011 km² in the first and last time intervals over the past four decades. Among nonwetland classes, the largest land cover transitions occurred between Grassland/Shrubland and Cropland areas, with the interchangeable conversion of about 31429 km² in total. Furthermore, Fig. 17 revealed that the Forest was also notably affected by land cover disturbances, including conversion to vegetated wetlands (VWs) (i.e., Bog, Fen, Swamp, and Marsh) with an area of approximately 17132 km². Additionally, 1300 km² and 2621 km² of Forest were converted to Barren and Cropland due to AN activities, such as deforestation due to fire events (e.g., human fire and wildfire), infrastructure

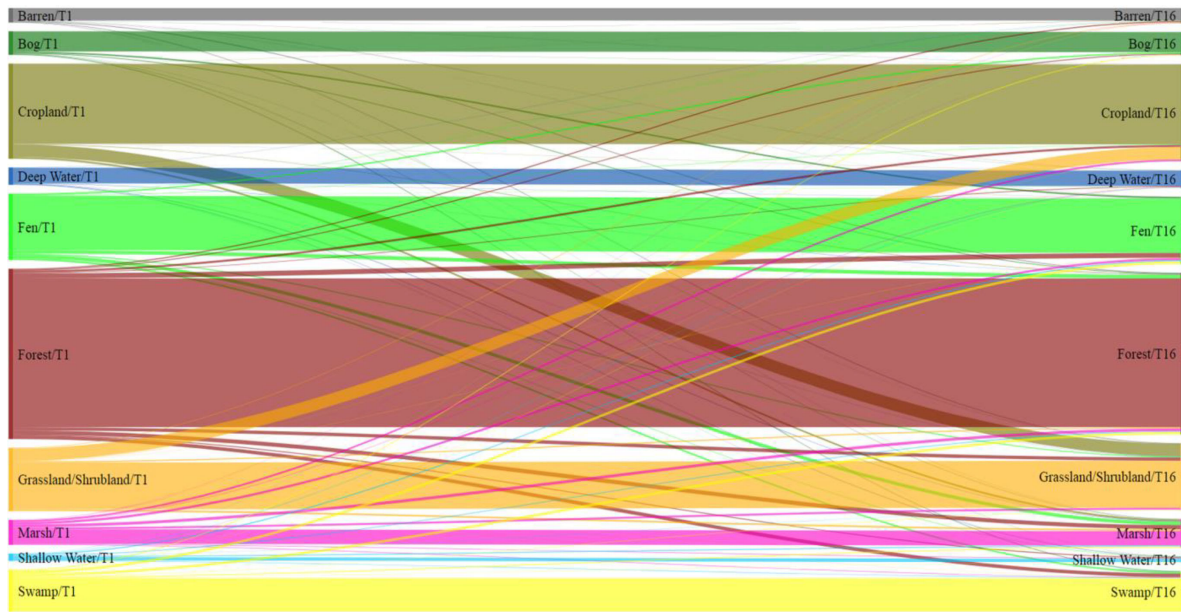


Fig. 17. Sankey diagram of transitions between different classes. Each line represents the transition between each pair of classes from T1 (first wetland map) to T16 (last wetland map). The thicker the lines, the higher the area of transition.

TABLE V
FROM/TO MATRIX BASED ON THE AREAS OF THE CLASSES KM² BETWEEN 1984 AND 2020

1984-1986	2019-2020											Total (%)
	Barren	Bog	Cropland	Deep Water	Fen	Forest	Grassland/Shrubland	Marsh	Shallow Water	Swamp	Total	
Barren	15,686.4	22.2	201.6	283.7	203.6	842	664.5	204.2	74.6	29.8	18,212.6	2.75
Bog	62.2	25,390.3	92.8	45.9	1,884.9	833.3	210.4	425.9	76.7	775.3	29,797.7	4.50
Cropland	255.2	8.7	100,896.2	204.2	123.0	585.5	15,590.8	2,321.0	98.1	15.2	120,097.9	18.12
Deep Water	222.3	16.5	93.1	19,499.6	231.1	330.4	254.2	636.7	517.4	124.7	21,926.0	3.31
Fen	381.4	1,770.2	492.1	201.2	68,398.8	4,505.3	1,272.7	4,186.3	541.8	2,057.9	83,807.7	12.65
Forest	1,300.7	1,144.3	2,621.6	742.4	6,328.8	187,741.3	4,292.5	5,094.6	1,083.0	4,566.6	214,915.8	32.43
Grassland/Shrubland	677.8	20.1	15,839.0	225.1	344.9	1,463.7	59,005.8	2,266.0	110.1	64.4	80,016.9	12.08
Marsh	256.3	145.1	227.1	407.5	2,748.5	3,493.0	2474	18,444.4	631.4	628.5	31,499.7	4.75
Shallow Water	116.3	87.2	70.6	467.5	1,298.6	935.2	301.1	1,090.1	4,283.1	627.2	9,276.9	1.40
Swamp	146.6	1,039.3	222.8	279.7	34,49.9	3,258.3	622.6	1,355.6	345.3	42,388.3	53,108.4	8.01
Total	19,105.2	29,643.9	122,800.8	22,355.9	85,012.1	203,988	84,688.6	36,024.8	7,761.5	51,277.9	662,658.7	100
Total (%)	2.88	4.47	18.53	3.37	12.83	30.78	12.78	5.44	1.17	7.74	100	

development, and agricultural encroachment. Fig. 17 also reflects the land cover transitions between different VW classes, which can be the result of the natural process due to climate change that exerts considerable influence over the governing ecosystem functionality and characteristics of wetlands. In this regard, Fen was subjected to a higher rate of transition to Bog (1770 km²), Marsh (4186 km²), and Swamp (2057 km²). However, the Fen class was increased from land cover conversions of the Forest and Swamp classes by approximately 6328 km² and 3449 km², respectively. In the second place, Swamp was also converted to other VWs with a total area of 5843 km².

Based on the results provided in Fig. 17 and Table V, the major reason for wetland changes was associated with the transition between different wetland classes and accounted for

about 19062 km². For instance, Fen was subjected to substantial transition to other wetland classes of Bog, Marsh, and Swamp by approximately 8013 km². This considerable transition was due to two reasons: 1) wetlands' natural succession; and 2) classification errors due to spectral similarity of wetland classes. For instance, most peatlands start developing as Fen and, then, they are eventually converted to Bog due to long-term peat accumulation [64]. Likewise, the continuous drying condition as a result of temperature rise and precipitation deficiency prepares the required condition for woody vegetation growth over time, leading to conversion of Fen/Bog to Swamp [64]. Similarly, with regards to the hydrosere succession, as a frequently autogenic natural succession, Marsh areas are to be converted to peatlands (i.e., ombrotrophic and minerotrophic) of Bog and Fen due to

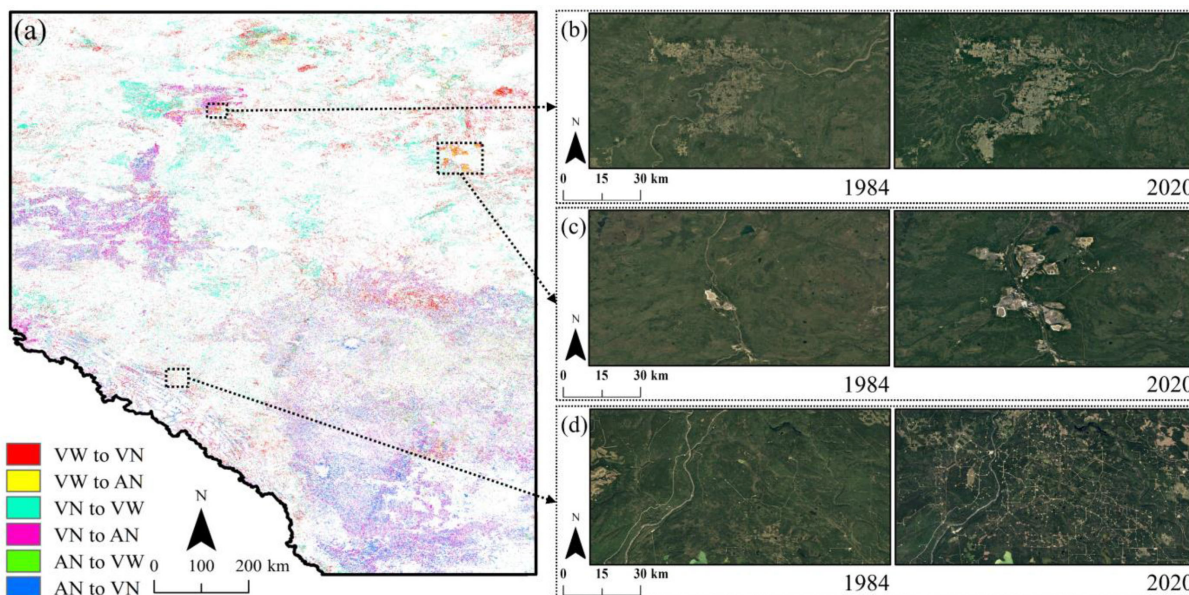


Fig. 18. (a) Spatial distribution of land cover transition based on the Category-2 classes (see Table II). (b)–(d) The sample satellite images over different areas with land cover transition between 1984 and 2020 (VW, VN, and AN).

organic and mineral materials accumulation [65], [66]. The latter reason is caused by the spectral similarity between different wetland classes. For instance, a notable confusion was found between the Bog from Fen classes (see Table IV) since these two wetlands are ecologically similar [67].

The transition between classes was also assessed based on classes of Category-2 (see Table II), where the results are illustrated in Fig. 18. The biggest conversion occurred between the VN class and two other classes, which in total accounted for 39 765 km². The conversion of the VN class was specifically associated with human-induced activities, such as deforestation and agricultural expansion. For instance, Fig. 18(d) shows the satellite images from 1984 and 2020, in which well sites development resulted in the loss of VN (e.g., Forest) and VW (e.g., Bog, Fen, and Swamp) areas. Similarly, the VN transition to AN (i.e., deforestation) occurred due to agricultural expansion, as shown in Fig. 18(b). Furthermore, the VW class was also subjected to a substantial change of approximately 16 958 km² to VN. Likewise, nearly 3847 km² of VW was converted to AN, resulting from possible wetland drainage for agricultural purposes. Fig. 18(c) shows the tailing pond developments that caused a loss of VW, especially the Swamp and Fen classes. Additionally, over the past four decades, AN was mostly changed to VN with an area of about 16 512 km² that can be linked to land reclamation purposes, such as afforestation. In particular, such a map [see Fig. 18(a)] can be efficiently applied to monitor and certify the land cover reclamations (i.e., adjusting soil layers and tree planting) over the oil sands sites, which are established by causing VW and VN disturbances.

5) *Land Cover Consistency*: Finally, to determine the stability of the class label of pixels within the study period, a consistency map was produced and illustrated in Fig. 19. In this regard, all 16 wetland maps were processed to generate the consistency map, which can be used as a sophisticated change indicator. The consistency map values varied between 0 and 15,

TABLE VI
DEFINED CONSISTENCY CLASSES WITH THEIR CORRESPONDING CONSISTENCY VALUES AND AREA

Class	Consistency values	Area (km ²)
Very-high	1-3	148,715
High	4-6	17,245
Medium	7-9	2,751
Low	10-12	317
Very-Low	13-15	5

in which 0 means that the corresponding pixel has not changed in the last four decades, and 15 implies that the considered pixel has changed in all time intervals. Generally, in most cases, which accounted for nearly 78.12%, only 1 or 2 changes in the labels of classes have occurred for pixels and can be inferred via visual inspection of Fig. 19(a). Furthermore, to provide an enhanced overview of the consistency of the land cover anomalies, the consistency map was classified into five classes.

- 1) Very-high.
- 2) High.
- 3) Medium.
- 4) Low.
- 5) Very-low.

Very-high indicates that these pixels had higher stability than others. The classified consistency map and areas of each class, along with corresponding consistency values, are provided in Fig. 19(b) and Table VI, respectively. It was found that several locations were among Low and Very-low classes, in which land cover labels experienced high oscillation. Further investigations showed that these high fluctuations were associated with three reasons.

- 1) Change between the deep water and shallow water class.
- 2) Change between the marsh and shallow water classes.
- 3) Misclassification error between the swamp and forest classes.

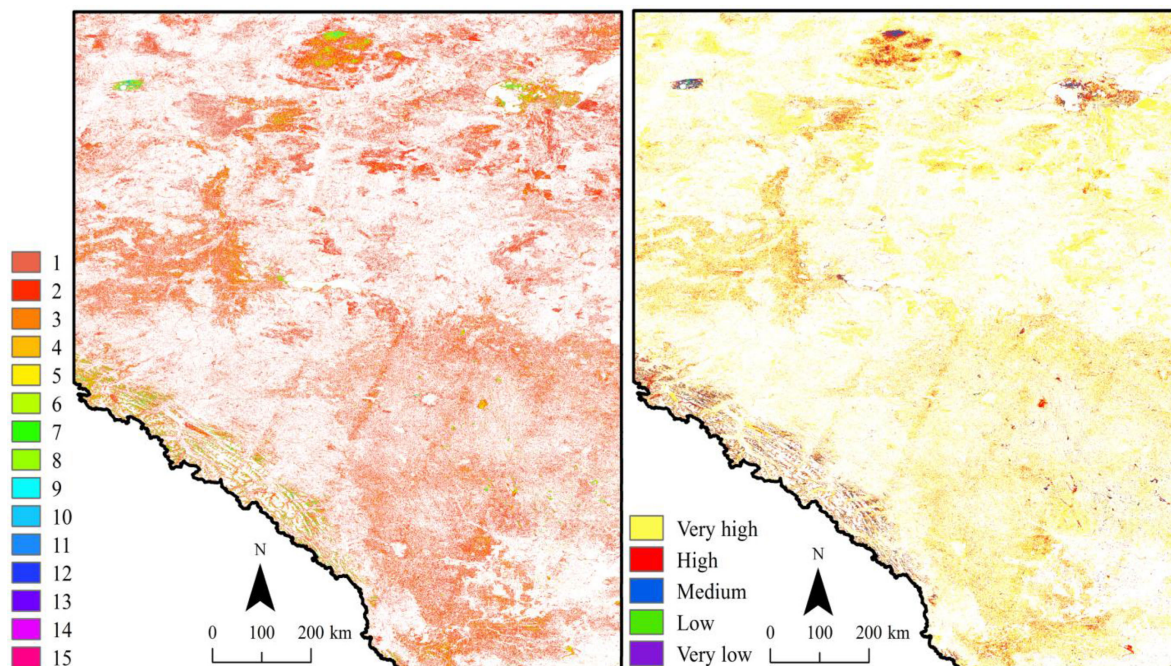


Fig. 19. (a) Consistency map and (b) the classified consistency map based on classes of Table VI, generated by employing 16 wetland maps over the past four decades.

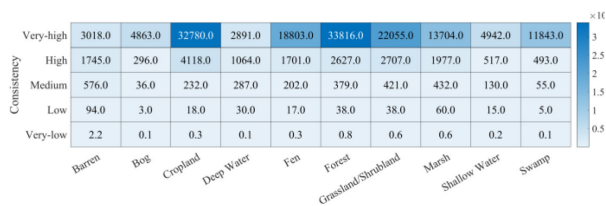


Fig. 20. Heat map generated by integrating the first wetland and the classified consistency maps to reveal the stability of different classes over the last four decades (values indicate the area of classes in km²).

The first was most probably linked to the water level alteration in different time intervals and alteration in water properties (e.g., turbidity and algal bloom) that caused the algorithm to misclassify the corresponding pixel to either Deep Water or Shallow Water alternatively. In particular, Deep Water was surrounded by Shallow Water, and the change of their discriminating boundary introduced such misclassification. The second was mainly related to the existence/abundance of different vegetated areas in the water (e.g., emergent marsh), which led to the misclassification between Marsh and Shallow Water. The latter was also related to the classification error in discriminating Swamp and Forest due to the spectral similarity of these two classes in optical satellite data. Based on Table VI, almost 87.97% of the pixels were assigned to Very-high that only experienced 1–3 land cover shifts, while a small portion (0.20%) of pixels were classified as Low and Very-low.

Finally, the first wetland map and the classified consistency map were integrated to identify the most stable classes over the past four decades. Fig. 20 presents the heat map generated from this combination. Based on the provided heat map, Cropland and Forest classes were the most stable, respectively, which can also be related to their large coverage in Alberta. Moreover, Fen

was the most consistent among the wetland classes, with an area of about 33 815 km². Additionally, two classes of Barren and Marsh with areas of approximately 6 722 km² and 4 926 km² were the most unstable classes over the last four decades.

V. SUGGESTIONS FOR FUTURE STUDIES

Due to the acknowledged efficacy and high potential of the RF classifier for wetland mapping [54], [55], an RF classifier was employed to generate 16 wetland maps of Alberta between 1984 and 2020. The non-parametric characteristics, resistance to noise and overfitting issues, high-computational efficiency for large-scale mapping, as well as providing accurate classification results make the RF a beneficial classifier for this task [10], [68]. The obtained overall accuracies and KCs (see Fig. 7) of all wetland maps also proved the capability of the RF for large-scale wetland mapping and CD. However, since a large number of permanent reference samples are available for Alberta, other sophisticated and state-of-the-art deep neural networks algorithms can be implemented in future works for wetland change analysis to produce more accurate results.

In this study, Landsat archive (i.e., Landsat 5, 7, and 8) datasets were employed for wetland mapping and CD. This was because Landsat archive is the only option when the objective is CD over a very long period (e.g., four decades). However, the medium spatial resolution of the imagery collected by the Landsat series can be an inherent source of misclassification and errors in the wetland change analyses. For instance, separation of the Swamp and Forest classes is a challenging task without the use of Synthetic Aperture Radar (SAR) data. In fact, these two woody vegetation and treed areas possess similar spectral signatures and, thus, SAR data with longer wavelength (e.g., L-band) is required to precisely separate these classes. This is rooted in the fact that

SAR data can penetrate from the vegetation canopy of trees and capture discriminative information about the low-lying lands of Swamp and Forest [1]. Unfortunately, there is no long-term SAR data available that can be integrated with the Landsat archive to empower the classifier for long-term wetland mapping and CD. However, if the objective is shorter-term wetland CD, open-access Sentinel-1/2 and RADARSAT datasets can be effectively utilized. Moreover, as the results suggested, the high confusion between Bog and Fen causes several uncertainties and, thus, in future studies, these classes may be integrated as a peatland class to improve the reliability of results. Additionally, the dynamic characteristics of wetlands and their seasonal variabilities could also affect the CD results and be regarded as other sources of errors. In fact, the dynamic interaction of wetlands with the surrounding environments causes wetland features, including water, vegetation, and chemical characteristics, to change over time and, thus, they may look different over years and months. Furthermore, the variation in the number of images in each time interval might also be considered another source of error. This is because each time interval included images with different dates and, thus, the image compositions were modestly different.

Finally, considering all the advantages of this study, such as the high classification accuracies and robust advanced RS and machine learning models, it is recommended to evaluate the developed models over the other Canadian provinces or the entire country.

VI. CONCLUSION

Wetlands in Alberta have been negatively affected by various natural and AN disturbances over the past decades. In this study, a long-term wetland change analysis (37 years) was conducted in Alberta to provide comprehensive information about the wetland gain and loss, as well as transitions between wetland and non-wetland classes. In total, 16 wetland maps were first produced from 1984 to 2020. It was observed that all the produced maps had a high quality in terms of visual assessment. Moreover, the OAs and class accuracies (i.e., PAs and UAs) of all maps were generally above 87% and 80%, respectively.

Additionally, various change analyses based on the produced 16 wetland maps were conducted. The results showed that 18.25% (120919 km²) and 81.75% (541734 km²) of the province have been changed and remained unchanged over the past four decades, respectively. The highest changes were over the north and north-east areas, as well as oil sands regions, where there was a significant decrease in the amount of Forest (from 214915 km² in 1984 to 203987 km² in 2020). In terms of the wetland classes, the decreasing and increasing trends were observed for the Shallow Water and March classes, respectively. However, the trends for the Bog, Fen, and Swamp were relatively stable. The results of gain and loss for only the wetland classes also showed that the biggest gain and loss were for the Marsh and Fen classes, respectively, while the lowest gain and loss were for the Shallow Water and Bog classes, respectively. Furthermore, it was observed that there was a significant transition between the Cropland and Grassland/Shrubland classes over the period of this study. There was also a considerable transition from the Forest class to other wetland and nonwetland classes, indicating the significant amount of deforestation in the province.

The satisfactory results of this study proved the applicability of the proposed approach for CD analysis in Canada. Therefore,

it is believed that the adopted CD approach can be integrated with other complementary data (i.e., field surveys) for profound investigations over the intensified changed areas of oil sand regions. Therefore, it is of great importance to employ advanced RS technologies for continuous and near-real-time monitoring of these regions. Additionally, the methodology presented in this study can be applied to investigate the success of landscape reclamation in Alberta, especially over oil sand regions. In conclusion, the analyses performed in this study are valuable for monitoring wetlands in Canada, which contain ~24% of the global wetlands and preventing these natural resources monitoring.

ACKNOWLEDGMENT

The authors would like to appreciate Dr. L. Chasmer's valuable comments in this article.

REFERENCES

- [1] S. Mahdavi, B. Salehi, J. Granger, M. Amani, B. Brisco, and W. Huang, "Remote sensing for wetland classification: a comprehensive review," *GISci. Remote Sens.*, vol. 55, no. 5, pp. 623–658, Sep. 2018, doi: [10.1080/15481603.2017.1419602](https://doi.org/10.1080/15481603.2017.1419602).
- [2] J. K. Pattison-Williams, J. W. Pomeroy, P. Badiou, and S. Gabor, "Wetlands, flood control and ecosystem services in the smith creek drainage basin: A case study in saskatchewan, Canada," *Ecol. Econ.*, vol. 147, pp. 36–47, May 2018, doi: [10.1016/j.ecolecon.2017.12.026](https://doi.org/10.1016/j.ecolecon.2017.12.026).
- [3] F. Parish and C. Looi, "Wetlands, biodiversity and climate change," Options and needs for enhanced linkage between the Ramsar convention on wetlands, Convention on Biological Diversity and UN Framework Convention on Climate Change, 1999.
- [4] M. Koch, T. Schmid, M. Reyes, and J. Gumuzzio, "Evaluating full polarimetric C-and L-band data for mapping wetland conditions in a semi-arid environment in Central Spain," *IEEE J. Sel. Top. Appl. Earth Observ. Remote Sens.*, vol. 5, no. 3, pp. 1033–1044, Jun. 2012.
- [5] W. J. Mitsch and J. G. Gosselink, *Wetlands*. New York, NY, USA: Wiley, 2000.
- [6] A. J. Green *et al.*, "Creating a safe operating space for wetlands in a changing climate," *Front. Ecol. Environ.*, vol. 15, no. 2, pp. 99–107, 2017.
- [7] N. Gorelick, M. Hancher, M. Dixon, S. Ilyushchenko, D. Thau, and R. Moore, "Google Earth Engine: Planetary-scale geospatial analysis for everyone," *Remote Sens. Environ.*, vol. 202, pp. 18–27, Dec. 2017, doi: [10.1016/j.rse.2017.06.031](https://doi.org/10.1016/j.rse.2017.06.031).
- [8] M. Amani *et al.*, "Google earth engine cloud computing platform for remote sensing big data applications: A comprehensive review," *IEEE J. Sel. Top. Appl. Earth Observ. Remote Sens.*, vol. 13, pp. 5326–5350, 2020.
- [9] M. Mahdianpari *et al.*, "A large-scale change monitoring of wetlands using time series Landsat imagery on Google Earth Engine: A case study in Newfoundland," *GISci. Remote Sens.*, vol. 57, no. 8, pp. 1102–1124, Nov. 2020, doi: [10.1080/15481603.2020.1846948](https://doi.org/10.1080/15481603.2020.1846948).
- [10] A. Ghorbanian, M. Kakooei, M. Amani, S. Mahdavi, A. Mohammadzadeh, and M. Hasanlou, "Improved land cover map of Iran using Sentinel imagery within Google Earth Engine and a novel automatic workflow for land cover classification using migrated training samples," *ISPRS J. Photogramm. Remote Sens.*, vol. 167, pp. 276–288, 2020, doi: [10.1016/j.isprsjprs.2020.07.013](https://doi.org/10.1016/j.isprsjprs.2020.07.013).
- [11] M. Mahdianpari *et al.*, "Big data for a big country: The first generation of Canadian wetland inventory map at a spatial resolution of 10-m using Sentinel-1 and Sentinel-2 data on the Google earth engine cloud computing platform," *Can. J. Remote Sens.*, vol. 46, no. 1, pp. 15–33, Jan. 2020, doi: [10.1080/07038992.2019.1711366](https://doi.org/10.1080/07038992.2019.1711366).
- [12] A. Naboureh, H. Ebrahimi, M. Azadbakht, J. Bian, and M. Amani, "RUESVMs: An ensemble method to handle the class imbalance problem in land cover mapping using Google Earth Engine," *Remote Sens.*, vol. 12, no. 21, Oct. 2020, Art.no. 3484, doi: [10.3390/rs12213484](https://doi.org/10.3390/rs12213484).
- [13] A. Ghorbanian, S. Zaghian, R. M. Asiyabi, M. Amani, A. Mohammadzadeh, and S. Jamali, "Mangrove ecosystem mapping using Sentinel-1 and Sentinel-2 satellite images and random forest algorithm in Google Earth Engine," *Remote Sens.*, vol. 13, no. 13, Jun. 2021, Art. no. 2565, doi: [10.3390/rs13132565](https://doi.org/10.3390/rs13132565).

- [14] J. Xiong *et al.*, "Automated cropland mapping of continental Africa using Google Earth Engine cloud computing," *ISPRS J. Photogramm. Remote Sens.*, vol. 126, pp. 225–244, 2017.
- [15] M. Amani *et al.*, "Application of Google Earth Engine cloud computing platform, sentinel imagery, and neural networks for crop mapping in Canada," *Remote Sens.*, vol. 12, no. 21, 2020, Art. no. 3561.
- [16] K. Ivushkin, H. Bartholomeus, A. K. Bregt, A. Pulatov, B. Kempen, and L. de Sousa, "Global mapping of soil salinity change," *Remote Sens. Environ.*, vol. 231, Sep. 2019, Art. no. 111260, doi: [10.1016/j.rse.2019.111260](https://doi.org/10.1016/j.rse.2019.111260).
- [17] R. Goldblatt, W. You, G. Hanson, and A. Khandelwal, "Detecting the boundaries of urban areas in India: A dataset for pixel-based image classification in Google Earth Engine," *Remote Sens.*, vol. 8, no. 8, Aug. 2016, Art. no. 634, doi: [10.3390/rs8080634](https://doi.org/10.3390/rs8080634).
- [18] D. Scherler, H. Wulf, and N. Gorelick, "Global assessment of supraglacial debris-cover extents," *Geophys. Res. Lett.*, vol. 45, no. 21, pp. 11,798–11,805, Nov. 2018, doi: [10.1029/2018GL080158](https://doi.org/10.1029/2018GL080158).
- [19] T. He, W. Xiao, Y. Zhao, X. Deng, and Z. Hu, "Identification of water-logging in Eastern China induced by mining subsidence: A case study of Google earth engine time-series analysis applied to the Huainan coal field," *Remote Sens. Environ.*, vol. 242, Jun. 2020, Art. no. 111742, doi: [10.1016/j.rse.2020.111742](https://doi.org/10.1016/j.rse.2020.111742).
- [20] J. - F. Pekel, A. Cottam, N. Gorelick, and A. S. Belward, "High-resolution mapping of global surface water and its long-term changes," *Nature*, vol. 540, no. 7633, pp. 418–422, Dec. 2016, doi: [10.1038/nature20584](https://doi.org/10.1038/nature20584).
- [21] M. Fuentes, K. Millard, and E. Laurin, "Big geospatial data analysis for Canada's Air Pollutant Emissions Inventory (APEI): Using google earth engine to estimate particulate matter from exposed mine disturbance areas," *GIScience Remote Sens.*, vol. 57, no. 2, pp. 245–257, Feb. 2020, doi: [10.1080/15481603.2019.1695407](https://doi.org/10.1080/15481603.2019.1695407).
- [22] W. Chen, H. Wang, H. Zhao, and K. Qin, "Google earth engine-assisted black carbon radiative forcing calculation over a heavy industrial city in China," *Air Qual. Atmos. Health*, vol. 13, no. 3, pp. 329–338, Mar. 2020, doi: [10.1007/s11869-020-00796-9](https://doi.org/10.1007/s11869-020-00796-9).
- [23] Y. Chen *et al.*, "Effects of reclamation and natural changes on coastal wetlands bordering China's Yellow Sea from 1984 to 2015," *Land Degrad. Dev.*, vol. 30, no. 13, pp. 1533–1544, 2019.
- [24] M. C. Hansen *et al.*, "High-resolution global maps of 21st-century forest cover change," *Science*, vol. 342, no. 6160, pp. 850–853, Nov. 2013, doi: [10.1126/science.1244693](https://doi.org/10.1126/science.1244693).
- [25] A. Midekisa *et al.*, "Mapping land cover change over continental Africa using Landsat and Google Earth Engine cloud computing," *PLoS One*, vol. 12, no. 9, Sep. 2017, Art. no. e0184926, doi: [10.1371/journal.pone.0184926](https://doi.org/10.1371/journal.pone.0184926).
- [26] K. Shimizu, T. Ota, and N. Mizoue, "Detecting forest changes using dense Landsat 8 and Sentinel-1 time series data in tropical seasonal forests," *Remote Sens.*, vol. 11, no. 16, Aug. 2019, Art. no. 1899, doi: [10.3390/rs11161899](https://doi.org/10.3390/rs11161899).
- [27] C. Huang, J. Yang, H. Lu, H. Huang, and L. Yu, "Green spaces as an indicator of urban health: Evaluating its changes in 28 mega-cities," *Remote Sens.*, vol. 9, no. 12, Dec. 2017, Art. no. 1266, doi: [10.3390/rs9121266](https://doi.org/10.3390/rs9121266).
- [28] V. - E. Neageo, R. - M. Stoica, A. - I. Ciurea, L. Bruzzone, and F. Bovolo, "Concurrent self-organizing maps for supervised/unsupervised change detection in remote sensing images," *IEEE J. Sel. Top. Appl. Earth Obs. Remote Sens.*, vol. 7, no. 8, pp. 3525–3533, Aug. 2014.
- [29] A. Moghimi, A. Mohammadzadeh, C. Turgay, and M. Amani, "A novel radiometric control set sample selection strategy for relative radiometric normalization of multitemporal satellite images," *IEEE Trans. Geosci. Remote Sens.*, vol. 59, no. 3, pp. 2503–2519, Mar. 2021.
- [30] M. Hussain, D. Chen, A. Cheng, H. Wei, and D. Stanley, "Change detection from remotely sensed images: From pixel-based to object-based approaches," *ISPRS J. Photogramm. Remote Sens.*, vol. 80, pp. 91–106, Jun. 2013, doi: [10.1016/j.isprsjprs.2013.03.006](https://doi.org/10.1016/j.isprsjprs.2013.03.006).
- [31] A. Almutairi and T. A. Warner, "Change detection accuracy and image properties: A study using simulated data," *Remote Sens.*, vol. 2, no. 6, pp. 1508–1529, Jun. 2010, doi: [10.3390/rs2061508](https://doi.org/10.3390/rs2061508).
- [32] A. Moghimi, A. Mohammadzadeh, and S. Khazai, "Integrating thresholding with level set method for unsupervised change detection in multitemporal SAR images," *Can. J. Remote Sens.*, vol. 43, no. 5, pp. 412–431, Sep. 2017, doi: [10.1080/07038992.2017.1342205](https://doi.org/10.1080/07038992.2017.1342205).
- [33] A. P. Tewkesbury, A. J. Comber, N. J. Tate, A. Lamb, and P. F. Fisher, "A critical synthesis of remotely sensed optical image change detection techniques," *Remote Sens. Environ.*, vol. 160, pp. 1–14, 2015.
- [34] S. T. Seydi, M. Hasanlou, and M. Amani, "A new end-to-end multi-dimensional CNN framework for land cover/land use change detection in multi-source remote sensing datasets," *Remote Sens.*, vol. 12, no. 12, Jun. 2020, Art. no. 2010, doi: [10.3390/rs12122010](https://doi.org/10.3390/rs12122010).
- [35] S. Mahdavi, B. Salehi, W. Huang, M. Amani, and B. Brisco, "A PolSAR change detection index based on neighborhood information for flood mapping," *Remote Sens.*, vol. 11, no. 16, 2019, Art. no. 1854.
- [36] Alberta Wilderness Association, "A wetland is the general term we use to describe parts of the landscape where water and land meet and intermingle," Accessed: Aug. 2020. [Online]. Available: <https://albertawilderness.ca/issues/wildwater/wetlands/>
- [37] T. Grabs, J. Seibert, K. Bishop, and H. Laudon, "Modeling spatial patterns of saturated areas: A comparison of the topographic wetness index and a dynamic distributed model," *J. Hydrol.*, vol. 373, no. 1/2, pp. 15–23, Jun. 2009, doi: [10.1016/j.jhydrol.2009.03.031](https://doi.org/10.1016/j.jhydrol.2009.03.031).
- [38] S. N. Gillanders, N. C. Coops, M. A. Wulder, and N. R. Goodwin, "Application of Landsat satellite imagery to monitor land-cover changes at the Athabasca Oil Sands, Alberta, Canada," *Can. Geogr. /Le Géographe Can.*, vol. 52, no. 4, pp. 466–485, Dec. 2008, doi: [10.1111/j.1541-0064.2008.00225.x](https://doi.org/10.1111/j.1541-0064.2008.00225.x).
- [39] S. Clare and I. F. Creed, "Tracking wetland loss to improve evidence-based wetland policy learning and decision making," *Wetlands Ecol. Manage.*, vol. 22, no. 3, pp. 235–245, Jun. 2014, doi: [10.1007/s11273-013-9326-2](https://doi.org/10.1007/s11273-013-9326-2).
- [40] V. C. Hawkes, M. T. Miller, J. Novoa, E. Ibeke, and J. P. Martin, "Opportunistic wetland formation, characterization, and quantification on landforms reclaimed to upland ecosites in the Athabasca Oil Sands Region," *Wetlands Ecol. Manage.*, vol. 28, no. 6, pp. 953–970, Dec. 2020, doi: [10.1007/s11273-020-09760-x](https://doi.org/10.1007/s11273-020-09760-x).
- [41] Alberta Biodiversity Monitoring Institute, "Biodiversity in Alberta," 2019. [Online]. Available: <https://www.abmi.ca/home/biodiversity/biodiversity-in-alberta.html>
- [42] X. Guo, N. C. Coops, P. Tompalski, S. E. Nielsen, C. W. Bater, and J. J. Stadt, "Regional mapping of vegetation structure for biodiversity monitoring using airborne LiDAR data," *Ecol. Informat.*, vol. 38, pp. 50–61, 2017.
- [43] D. J. Downing and W. W. Pettapiece, "Natural regions and subregions of Alberta," 2006, Natural Regions Committee.
- [44] Alberta WaterPortal Society, "Climate in Alberta," Accessed: Aug. 2020. [Online]. Available: <https://albertawater.com/virtualwaterflows/climate-in-alberta>
- [45] Wetlands Alberta, "What is a wetland?," Accessed: Aug. 2020. [Online]. Available: <https://wetlandsalberta.ca/what-is-a-wetland/>
- [46] National Wetlands Working Group, *The Canadian Wetland Classification System*. Wetlands Res. Branch, Univ. Waterloo, Waterloo, ON, Canada, 1997.
- [47] S. Foga *et al.*, "Cloud detection algorithm comparison and validation for operational Landsat data products," *Remote Sens. Environ.*, vol. 194, pp. 379–390, 2017.
- [48] United States Geological Survey (USGS), "Landsat collection 1 level-1 quality assessment band," United States Geological Surv., 2020.
- [49] A. Ghorbanian and A. Mohammadzadeh, "An unsupervised feature extraction method based on band correlation clustering for hyperspectral image classification using limited training samples," *Remote Sens. Lett.*, vol. 9, no. 10, pp. 982–991, Oct. 2018, doi: [10.1080/2150704X.2018.1500723](https://doi.org/10.1080/2150704X.2018.1500723).
- [50] S. Mahdavi *et al.*, "Object-based classification of wetlands in Newfoundland and Labrador using multi-temporal PolSAR data," *Can. J. Remote Sens.*, vol. 43, no. 5, pp. 432–450, 2017.
- [51] M. Amani, B. Salehi, S. Mahdavi, J. E. Granger, B. Brisco, and A. Hanson, "Wetland classification using multi-source and multi-temporal optical remote sensing data in Newfoundland and Labrador, Canada," *Can. J. Remote Sens.*, vol. 43, no. 4, pp. 360–373, Jul. 2017, doi: [10.1080/07038992.2017.1346468](https://doi.org/10.1080/07038992.2017.1346468).
- [52] E. R. DeLancey, J. F. Simms, M. Mahdianpari, B. Brisco, C. Mahoney, and J. Kariyeva, "Comparing deep learning and shallow learning for large-scale wetland classification in Alberta, Canada," *Remote Sens.*, vol. 12, no. 1, Dec. 2019, Art. no. 2, doi: [10.3390/rs12010002](https://doi.org/10.3390/rs12010002).
- [53] R. Achanta and S. Susstrunk, "Superpixels and polygons using simple non-iterative clustering," in *Proc. IEEE Conf. Comput. Vis. Pattern Recognit.*, 2017, pp. 4895–4904, doi: [10.1109/CVPR.2017.520](https://doi.org/10.1109/CVPR.2017.520).
- [54] M. Amani, B. Salehi, S. Mahdavi, J. Granger, and B. Brisco, "Wetland classification in Newfoundland and Labrador using multi-source SAR and optical data integration," *GISci. Remote Sens.*, vol. 54, pp. 779–796, May 2017, doi: [10.1080/15481603.2017.1331510](https://doi.org/10.1080/15481603.2017.1331510).
- [55] M. Amani *et al.*, "Canadian wetland inventory using Google Earth Engine: The first map and preliminary results," *Remote Sens.*, vol. 11, no. 7, 2019, Art. no. 842, doi: [10.3390/rs11070842](https://doi.org/10.3390/rs11070842).
- [56] M. Amani *et al.*, "A generalized supervised classification scheme to produce provincial wetland inventory maps: an application of Google Earth Engine for big geo data processing," *Big Earth Data*, vol. 3, no. 4, pp. 378–394, 2019.

- [57] M. Amani *et al.*, "Evaluation of the landsat-based Canadian wetland inventory map using multiple sources: Challenges of large-scale wetland classification using remote sensing," *IEEE J. Sel. Top. Appl. Earth Obs. Remote Sens.*, vol. 14, pp. 32–52, Nov. 10, 2020, doi: [10.1109/JSTARS.2020.3036802](https://doi.org/10.1109/JSTARS.2020.3036802).
- [58] L. Chasmer, E. M. Lima, C. Mahoney, C. Hopkinson, J. Montgomery, and D. Cobbaert, "Shrub changes with proximity to anthropogenic disturbance in boreal wetlands determined using bi-temporal airborne LiDAR in the Oil Sands Region, Alberta Canada," *Sci. Total Environ.*, vol. 780, Aug. 2021, Art. no. 146638, doi: [10.1016/j.scitotenv.2021.146638](https://doi.org/10.1016/j.scitotenv.2021.146638).
- [59] C. Willier, "Changes in peatland plant community composition and stand structure due to road induced flooding and desiccation," Univ. Alberta, Edmonton, AB, Canada, 2017.
- [60] Alberta Agriculture and Forestry, Accessed: Aug. 2020. [Online]. Available: <https://wildfire.alberta.ca/resources/historical-data/spatial-wildfire-data.aspx>
- [61] L. E. Chasmer, C. D. Hopkinson, R. M. Petrone, and M. Sitar, "Using multitemporal and multispectral airborne lidar to assess depth of peat loss and correspondence with a new active normalized burn ratio for wildfires," *Geophys. Res. Lett.*, vol. 44, no. 23, pp. 11–851, 2017.
- [62] National Forestry Database, "Forest area burned and number of forest fires," Accessed: Aug. 2020. Online. [Available]: <https://cwfis.cfs.nrcan.gc.ca/ha/nfdb>
- [63] S. Chowdhury, D. R. Peddle, M. A. Wulder, S. Heckbert, T. C. Shipman, and D. K. Chao, "Estimation of land-use/land-cover changes associated with energy footprints and other disturbance agents in the Upper Peace Region of Alberta Canada from 1985 to 2015 using Landsat data," *Int. J. Appl. Earth Obs. Geoinf.*, vol. 94, Feb. 2021, Art. no. 102224, doi: [10.1016/j.jag.2020.102224](https://doi.org/10.1016/j.jag.2020.102224).
- [64] J. Loisel and M. Bunsen, "Abrupt Fen-Bog transition across southern patagonia: Timing, causes, and impacts on carbon sequestration," *Front. Ecol. Evol.*, vol. 8, Aug. 2020, doi: [10.3389/fevo.2020.00273](https://doi.org/10.3389/fevo.2020.00273).
- [65] P. Kuhry and J. Turunen, "The postglacial development of boreal and subarctic peatlands," in *Boreal Peatland Ecosystems*, vol. 188. Berlin, Germany: Springer, 2006, pp. 25–46. [Online]. Available: https://doi.org/10.1007/978-3-540-31913-9_3
- [66] M. Zobel, "Autogenic succession in boreal mires—A review," *Folia Geobot. Phytotaxon.*, vol. 23, no. 4, pp. 417–445, Dec. 1988, doi: [10.1007/BF02853361](https://doi.org/10.1007/BF02853361).
- [67] L. L. Bourgeau-Chavez *et al.*, "Mapping boreal peatland ecosystem types from multitemporal radar and optical satellite imagery," *Can. J. For. Res.*, vol. 47, no. 4, pp. 545–559, Apr. 2017, doi: [10.1139/cjfr-2016-0192](https://doi.org/10.1139/cjfr-2016-0192).
- [68] M. Belgiu and L. Drăguț, "Random forest in remote sensing: A review of applications and future directions," *ISPRS J. Photogramm. Remote Sens.*, vol. 114, pp. 24–31, Apr. 2016, doi: [10.1016/j.isprsjprs.2016.01.011](https://doi.org/10.1016/j.isprsjprs.2016.01.011).



Meisam Amani (Senior Member, IEEE) received the B.Eng. degree in geomatics engineering from the University of Tabriz, Tabriz, Iran, in 2012, the M.Eng. degree in remote sensing engineering from the K.N. Toosi University of Technology, Tehran, Iran, in 2014, and the Ph.D. degree in electrical engineering from the Memorial University of Newfoundland, St. John's, NL, Canada, in 2018.

He is currently a Senior Remote Sensing Engineer and the Key Specialty Leader of Data Analytics at a global consulting and engineering company, called

Wood PLC, where he manages and leads various industrial, governmental, and academic remote sensing projects worldwide. Over the past 11 years, he has worked on different applications of remote sensing, including but not limited to land cover/land use classification, soil moisture estimation, drought monitoring, water quality assessment, watershed management, power/transmission line monitoring, fog detection and nowcasting, and ocean wind estimation. To do these, he has utilized various remote sensing datasets (e.g., UAV, optical, LiDAR, SAR, scatterometer, radiometer, and altimeter) along with different machine learning and big data processing algorithms.

Dr. Amani is an Associate Editor in IEEE JSTARS and the Lead Guest Editor for a special issue in the Remote Sensing journal. He also serves as a regular reviewer in about 15 international remote sensing journals. He was the recipient of the prestigious Professional Engineers and Geoscientists Newfoundland and Labrador Environmental Award in 2020 due to his contribution to wetland mapping in Canada using advanced machine learning and big data processing algorithms. A list of his research works, including over 60 peer-reviewed journal and conference papers.



Sahel Mahdavi received the Ph.D. degree in electrical engineering from the Memorial University of Newfoundland, St. John's, NL, Canada, in 2018.

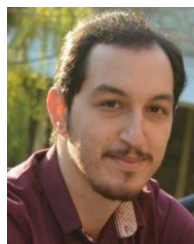
Having almost ten years of academic and industrial background in remote sensing, she is familiar with a wide array of topics relevant to RS/GIS and their applications in various environmental aspects. These topics include: object-based wetland classification using a combination of optical and full-polarimetric SAR data, feature selection, soil moisture retrieval using SAR images, image segmentation, speckle reduction in SAR images, target detection in multispectral optical images, and the relationship between environmental conditions and SAR images. She also coauthored a book entitled "Principles of SAR Remote Sensing". She has authored more than 40 peer-reviewed journals.

She was a Member of a provincial project on wetland classification during the Ph.D. when she identified the problem with wetland classification using remote sensing and, subsequently, proposed a novel scheme for wetland mapping. She is currently affiliated with the Data Analytics team at Wood PLC. She was the recipient of the Professional Engineers and Geoscientists Newfoundland and Labrador Environmental Award (2020), the Emera Graduate Scholarship for Distinctive Women in Engineering for three consecutive years (2016–2018), and Newfoundland and Labrador Branch of Canadian Institute of Geomatics (CIG) Scholarship (2015).



Mohammad Kakooei received the B.S., M.Sc., and Ph.D. degrees from the Shahid Beheshti University (SBU), Tehran, Iran, in 2011, the M.Sc. degree from the Iran University of Science and Technology (IUST), Tehran, Iran, in 2014, and the Ph.D. degree from Babol Noshirvani University of Technology (BNUT), Babol, Iran, in 2020, all in electronic engineering.

Then he became a Postdoc Researcher with the Department of Computer and Electrical Engineering, BNUT, Babol, Iran. He is currently a Researcher with the Department of Data Science and Artificial Intelligence, Chalmers University of Technology, Gothenburg, Sweden. His skills are not limited to a specific programming language and hardware, and he is qualified in programming from hardware- to software-level systems. He is experienced in programming in MATLAB, C/C++, Python, CUDA, and JavaScript. The implementation platforms vary from local systems to the cloud environment. To support remote sensing big data, he utilized the google earth engine platform in his recent research works considering near real-time earth surface monitoring, urban area analysis, building damage assessment, and wetland and cropland classification. His research interests include image processing, machine learning, remote sensing, parallel processing, GPGPU, and data mining applications.



Arsalan Ghorbanian received the B.Sc. degree in geodesy and geomatics and the M.Sc. degree in remote sensing from K. N. Toosi University of Technology, Tehran, Iran, in 2016 and 2018, respectively, where he is currently working toward the Ph.D. degree in remote sensing.

He serves as a reviewer in several international remote sensing journals and is currently a Guest Editor for a special issue in the Remote Sensing (MDPI) journal. His research interests include LULC mapping, geo-big data processing, satellite image and video processing, hyperspectral image processing, and soil moisture estimation from SAR data.



Brian Brisco received the Ph.D. degree in remote sensing/physical geography from the University of Kansas, Lawrence, KS, USA, in 1985, the M.Sc. degree in soil science, and the B.Sc. degree in ecology, both from the University of Guelph, Guelph, ON, Canada.

He is an internationally recognized authority on Synthetic Aperture Radar (SAR) and its application to a wide range of environmental monitoring applications.

He has been involved in remote sensing since 1975 and participated in the SURSAT project from 1977–1980 before spending four years with the Remote Sensing Laboratory, the University of Kansas under the supervision of Dr. F. T. Ulaby, widely recognized as one of the world's leading authorities on radar. He worked for Intera from 1989 until 1997 as a Research Associate after completion of an NSERC Postdoctoral fellowship served at the Canada Centre for Remote Sensing. Since 1997, he has been working for Noetix Research Inc. where he is the Director of Research and Applications Development. His research activities focus on using remote sensing, particularly synthetic aperture radar, for mapping and managing renewable resources. His extensive publications include studies on vegetation characterization, crop identification and monitoring, conservation farming/soil erosion mapping, soil moisture estimation, land cover mapping, wetland mapping, rangeland management, forestry, and developing tools and techniques for ground truth data acquisition. His work has included experience with interferometry, polarimetry, and radar backscatter modeling including software development and operational implementation. He has authored or coauthored more than 200 publications including more than 50 peer reviewed journal publications and is the author of two chapters in the Manual of Remote Sensing volume on radar applications published by ASPRS. He provides peer review services to all the major remote sensing journals and participates as an external examiner for many graduate students at various universities in Canada and abroad. He has been consulted or contracted by government and non-government organizations on a wide range of SAR applications and system development including NRCan, CSA, DND, AAFC, EC, NASA, ESA, NASDA, NOAA, USDA, CAS, etc. He has extensive contacts in the SAR community worldwide and has worked in China, Vietnam, Malaysia, Thailand, Indonesia, South Africa, Argentina, Uruguay, Chile, Brazil, Columbia, and Costa Rica. He is a Past-President of the Canadian Remote Sensing Society (CRSS) and the Canadian Aeronautics and Space Institute (CASI). His skills contribute to ESS Programs on remote sensing science, earth science for environment and health, enhancing resilience in a changing climate and northern resources and development.



Evan R. DeLancey received the Master of Science degree in remote sensing from the University of Alberta, Edmonton, AB, Canada, in 2014.

He is a Spatial Data Scientist with the Alberta Biodiversity Monitoring Institute with eight years of experience in remote sensing and GIS. He currently leads the Advanced Landcover Prediction and Habitat Assessment (ALPHA) program for the ABMI in Edmonton, Alberta, Canada. This program provides Landcover mapping and monitoring data for policy makers in government. Projects in this program include wetland inventory mapping for the province of Alberta, algal bloom monitoring with satellite data, and surface water dynamics. From this work, he has led or coauthored 15 scientific publications in the past five years.



Souleymane Toure received the first master's degree in physics and chemistry from the University of Abidjan, Abidjan, Côte d'Ivoire, 1994, the second master's degree in agrometeorology from the FUL University, Belgium, in 1996, and the third master's degree in remote sensing and cartography from the University of Louvain-La-Neuve, Ottignies-Louvain-la-Neuve, Belgium, in 2002, and the Ph.D. degree in environmental science and management from the University of Liège, Liège, Belgium, in 2004.

He has nearly 20 years of experience in management, teaching, research and development in the private, academia, and public sectors in Africa, Europe, and Canada. He is currently the Manager of Geospatial Data and Information Management Section, Canadian Wildlife Service, Environment and Climate Change Canada (ECCC), Gatineau, QC, Canada. He coordinates environmental programs and policies for assessment, stewardship, and wildlife planning, including fragile ecosystems, wetlands, migratory birds, and protected areas. He was a Researcher with the Department of Agriculture and Agri-Food for the development of agrienvironmental indicators (AEI) on soil, water and air quality, and design of landscape occupation models and their environmental impacts in agrometeorology. In 2008–2009, he was with the Ministry of the Environment, Province of Ontario, as the Natural Resources Manager and Contaminated Sites Monitor. From 2016 to 2018, he taught geomatics courses with the Department of Geography, University of Ottawa, and photogrammetry and geographical information system (GIS) with the Department of Forestry, Cit Collégiale in Ottawa.

Eugenio Landeiro Reyes is currently a Geomatics Technician with more than eight (+15) years of experience working with Geographic Information Systems (GIS) in the private and public sectors. Extensive experience using ArcGIS for geospatial data management (vector and raster). He managed and participated in projects related to geomatics, GIS, landscape and wetlands, risk, vulnerability, climate change and environmental studies while working in multidisciplinary teams. He has strong interpersonal skills, is an excellent team player, has the ability to work under pressure, is detail oriented, skilled in problem analysis and resolution. His research interests include, but not limited to, cartography, spatial analysis, validation, review, editing, correction, data management and research, and map design and creation supported by field work using GPS; database management; data modeling (model builder and Python), and geospatial analysis.